

Prior-preconditioned conjugate gradient method for accelerated Gibbs sampling in “large n & large p ” sparse Bayesian regression

Akihiko Nishimura and Marc A. Suchard

University of California - Los Angeles, USA

Summary. In a modern observational study based on healthcare databases, the number of observations and of predictors typically range in the order of $10^5 \sim 10^6$ and of $10^4 \sim 10^5$. Despite the large sample size, data rarely provide sufficient information to reliably estimate such a large number of parameters. Sparse regression techniques provide potential solutions, one notable approach being Bayesian methods based on shrinkage priors. In the “large n & large p ” setting, however, posterior computation encounters a major bottleneck at repeated sampling from a high-dimensional Gaussian distribution whose precision matrix Φ is expensive to compute and factorize. In this article, we present a novel algorithm to speed up this bottleneck based on the following observation: we can cheaply generate a random vector \mathbf{b} such that the solution to the linear system $\Phi\boldsymbol{\beta} = \mathbf{b}$ has the desired Gaussian distribution. We can then solve the linear system by the conjugate gradient (CG) algorithm through matrix-vector multiplications by Φ , without ever explicitly inverting Φ . We accelerate the convergence of CG in sparse regression applications by developing a theory of *prior-preconditioning*. We apply our algorithm to a clinically relevant large-scale observational study with $n = 72,489$ and $p = 22,175$, designed to assess the relative risk of adverse events from two alternative blood anti-coagulants. Our algorithm demonstrates an order of magnitude speed-up in the posterior computation.

Keywords: Conjugate gradient, Markov chain Monte Carlo, multivariate Gaussian, numerical linear algebra, sparse matrix, variable selection

1. Introduction

Given an outcome of interest y_i and a large number of features x_{i1}, \dots, x_{ip} for $i = 1, \dots, n$, the goal of sparse regression (or variable selection) is to find a small subset of these features that captures the principal relationship between the outcome and features. Such a sparsity assumption is mathematical necessity when p exceeds the sample size n . Even when $n > p$, however, the assumption often remains critical in improving the interpretability and stable estimation of regression coefficients $\boldsymbol{\beta}$. This is especially true under the following conditions, either of which reduces the amount of information the data provides on the regression coefficients:

- (a) the design matrix \mathbf{X} is sparse i.e. only a small fraction of the design matrix contains non-zero entries due to infrequently observed features.
- (b) the outcome \mathbf{y} is binary and imbalanced i.e. $y_i = 0$ (or $y_i = 1$) for most of i 's.

Sparse design matrices are extremely common in a modern observational study based on healthcare databases; while a large number of potential pre-existing conditions and available treatments exist, only a small subset of these applies to each patient (Schuemie et al., 2018b). Imbalanced binary outcomes are also common as many serious diseases of interest are rare among the population.

A particular application considered in this manuscript is a comparative study of two blood anti-coagulants *dabigatran* and *warfarin*, based on observational data from Truven Health MarketScan Medicare Supplemental and Coordination of Benefits Database. These drugs help prevent blood clot formation among patients with atrial fibrillation but come with risks of serious side effects. The goal of the study is to quantify which of the two drugs has a lower risk of intracranial hemorrhage (bleeding inside the skull) among treated patients. The data set consists of $n = 72,489$ patients and $p = 22,175$ predictors of potential relevance.

An increasingly common approach to sparse regression is the Bayesian method based on continuous shrinkage priors on the regression coefficients β . These priors often are represented as a scale-mixture of Gaussians

$$\beta_j | \lambda_j, \tau \sim \mathcal{N}(0, \tau^2 \lambda_j^2), \lambda_j \sim \pi_L(\cdot), \tau \sim \pi_T(\cdot), \quad (1.1)$$

with unknown *global scale* parameter τ and *local scale* parameter λ_j (Carvalho et al., 2010; Polson et al., 2014; Bhattacharya et al., 2015; Bhadra et al., 2017). Compared to more traditional “spike-and-slab” discrete-mixture priors for sparse Bayesian regression, these continuous shrinkage priors are typically more computationally efficient while maintaining highly desirable statistical properties (Bhattacharya et al., 2015; Pal et al., 2014; Datta et al., 2013). Despite the relative computational advantage, however, posterior inference under these priors still encounters a major scalability issue. For instance, for our comparative study of two anti-coagulants, it takes over 30 hours on 2015 iMac to run 1,000 iterations of the current state-of-the-art Gibbs sampler in our reasonably optimized Python implementation (Section 4).

In this article, we focus on accelerating the state-of-the-art Gibbs sampler for sparse Bayesian logistic regression, but our approach applies whenever the likelihood of the data or latent parameter can be expressed as a Gaussian mixture. The data augmentation scheme of Polson et al. (2013) makes a posterior under the logistic model amenable to Gibbs sampling as follows. Through a Polya-Gamma auxiliary parameter ω , the conditional likelihood of a binary outcome \mathbf{y} becomes

$$y'_i | \mathbf{X}, \beta, \omega \sim \mathcal{N}(x_i^\top \beta, \omega_i^{-1}) \text{ for } y'_i := \omega_i^{-1} (y_i - 1/2). \quad (1.2)$$

Correspondingly, the full conditional distribution of β is given by

$$\beta | \omega, \lambda, \tau, \mathbf{y}, \mathbf{X} \sim \mathcal{N}(\Phi^{-1} \mathbf{X}^\top \Omega \mathbf{y}', \Phi^{-1}) \text{ for } \Phi = \mathbf{X}^\top \Omega \mathbf{X} + \tau^{-2} \mathbf{\Lambda}^{-2}, \quad (1.3)$$

where $\Omega = \text{diag}(\omega)$, a diagonal matrix with entries $\Omega_{ii} = \omega_i$, and $\mathbf{\Lambda} = \text{diag}(\lambda)$. The main computational bottleneck of the Gibbs sampler arise from the need to sample from a high-dimensional Gaussian of the form (1.3). The standard algorithm requires $O(n^2 p + p^3)$ operations: $O(n^2 p)$ for computing the term $\mathbf{X}^\top \Omega \mathbf{X}$ for Φ and $O(p^3)$ for the Cholesky factorization of Φ . These operations remain significant

burden even with sparsity in \mathbf{X} because computation times of sparse linear algebra operations are dominated not by the number of arithmetic operations but by latency in irregular data access (Dongarra et al., 2016; Duff et al., 2017).

None of the recent computational advances addresses the “large n & large p ” logistic regression problem considered in this article. Significant progress has been made for $n \ll p$ cases by Bhattacharya et al. (2016), who propose an algorithm to sample from (1.3) with only $O(n^2p + n^3)$ operations. Johndrow et al. (2018) reduce the $O(n^2p)$ cost by replacing the matrix $\mathbf{X}\mathbf{\Lambda}^2\mathbf{X}^\top$ with an approximation that can be computed with $O(n^2k)$ operations for $k < p$. These techniques offer no reduction in computational cost for $n > p$ cases, however. Hahn et al. (2018) propose a sampling approach for linear regression based on an extensive pre-processing of the matrix $\mathbf{X}^\top\mathbf{X}$ — a trick limited in scope strictly to Gaussian likelihood models.

Proposed in this article is a novel algorithm to sample from a high-dimensional distribution of the form (1.3) through the conjugate gradient (CG) method, requiring only a small number of matrix-vector multiplications $\mathbf{v} \rightarrow \mathbf{\Phi}\mathbf{v}$. We can compute the vector $\mathbf{\Phi}\mathbf{v}$ without ever explicitly forming the matrix $\mathbf{\Phi}$; the only required operations are $\mathbf{v} \rightarrow \mathbf{X}\mathbf{v}$, $\mathbf{w} \rightarrow \mathbf{X}^\top\mathbf{w}$, and element-wise vector multiplications. This is an important feature when dealing with a large and sparse design matrix \mathbf{X} . The matrix $\mathbf{X}^\top\mathbf{\Omega}\mathbf{X}$ and hence $\mathbf{\Phi}$ typically contain a much larger proportion of non-zero entries than \mathbf{X} does, making it much more memory intensive to handle $\mathbf{\Phi}$ directly. For example, it requires 74.5 GB of memory to allocate a $p \times p$ dense matrix in double-precision numbers when $p = 10^5$. The ability to automatically exploits a sparsity structure in \mathbf{X} , therefore, is another major advantage of our algorithm.

Also developed is a theory of an effective *preconditioning* technique in the context of sparse Bayesian regression. Utility of CG depends critically on preconditioning, which improves the computational efficiency by relating a given problem to a modified one. Exploiting the fact that the shrinkage priors dominate likelihood for all but a small fraction of the regression coefficients, we develop what we term the *prior-preconditioning* approach and demonstrate its superiority over general-purpose preconditioners in sparse Bayesian regression applications.

The rest of the paper is organized as follows. Section 2 begins by describing how to recast the problem of sampling from the distribution (1.3) as that of solving a linear system $\mathbf{\Phi}\boldsymbol{\beta} = \mathbf{b}$, eliminating the need to compute and factorize $\mathbf{\Phi}$. The rest of the section explains how to apply CG to rapidly solve the linear system while developing theoretical foundations behind our prior preconditioner. In Section 3, we use simulated data to study the effectiveness of the CG-based sampler for sparse regressions. Also studied is how the behavior of CG depends on different preconditioning strategies. Finally, in Section 4, we apply our algorithm to carry out the dabigatran vs. warfarin comparison, demonstrating an order of magnitude speed-up in the posterior computation. Our CG-accelerated Gibbs sampler for sparse Bayesian logistic regression is implemented as the *bayesbridge* package available from Python Package Index (pypi.org). The source code is available at a GitHub repository <https://github.com/aki-nishimura/bayes-bridge>.

2. Conjugate gradient sampler for sparse regression posterior computation

2.1. Generating a Gaussian vector as the solution of a linear system

The standard algorithm for sampling a multivariate-Gaussian requires the Cholesky factorization $\Phi = \mathbf{L}\mathbf{L}^\top$ of its precision (or covariance) matrix (Rue and Held, 2005). When the precision matrix Φ has a specific structure as in (1.3), however, it turns out that the problem of sampling from the distribution (1.3) can be recast to that of solving a linear system. This in particular obviates the need to compute and factorize Φ . The key observation is that we can generate a Gaussian vector \mathbf{b} with $\text{Var}(\mathbf{b}) = \Phi$ for a computational cost negligible compared to the standard algorithm.

PROPOSITION 2.1. *The following procedure generates a sample β from distribution (1.3):*

- (a) *Generate $\mathbf{b} \sim \mathcal{N}(\mathbf{X}^\top \Omega \mathbf{y}', \Phi)$ by sampling independent Gaussian vectors $\boldsymbol{\eta} \sim \mathcal{N}(\mathbf{0}, \mathbf{I}_n)$ and $\boldsymbol{\delta} \sim \mathcal{N}(\mathbf{0}, \mathbf{I}_p)$ and then setting*

$$\mathbf{b} = \mathbf{X}^\top \Omega \mathbf{y}' + \mathbf{X}^\top \Omega^{1/2} \boldsymbol{\eta} + \tau^{-1} \mathbf{\Lambda}^{-1} \boldsymbol{\delta}. \quad (2.4)$$

- (b) *Solve the following linear system for β :*

$$\Phi \beta = \mathbf{b} \quad (\text{where } \Phi = \mathbf{X}^\top \Omega \mathbf{X} + \tau^{-2} \mathbf{\Lambda}^{-2}). \quad (2.5)$$

The result follows immediately from basic properties of multivariate Gaussians; in particular, the solution to (2.5) has the required covariance structure because $\text{Var}(\Phi^{-1} \mathbf{b}) = \Phi^{-1} \text{Var}(\mathbf{b}) (\Phi^{-1})^\top$.

The above algorithm complements the algorithm Bhattacharya et al. (2016) propose; their algorithm reduces the task of sampling a multivariate Gaussian to solving a $n \times n$ linear system, while our algorithm reduces it to solving a $p \times p$ system.

2.2. Iterative method for solving a linear system

Proposition 2.1 is useful because solving the linear system (2.5) can be significantly faster than the standard algorithm for sampling a Gaussian vector. We achieve this speed-up by applying the CG method (Hestenes and Stiefel, 1952; Lanczos, 1952). CG belongs to a family of *iterative methods* for solving a linear system. Compared to traditional direct methods, iterative methods are more memory efficient and, if the matrix Φ has certain structures (Section 2.3), can be significantly faster.

Iterative methods have found applications in Gaussian process models, where optimizing the hyper parameters of covariance functions requires solving linear systems involving large covariance matrices (Gibbs and MacKay, 1996). Significant research has gone into how best to apply iterative methods in this specific context; see Stein et al. (2012), Sun and Stein (2016), and Stroud et al. (2017) for example. Outside the Gaussian process literature, Zhou and Guan (2017) use an iterative method to address the bottleneck of having to solve large linear systems when computing Bayes factors in a model selection problem.

A novel feature of our work is the use of CG as a computational tool for Monte Carlo simulation. A related work is Zhang et al. (2018), brought to our attention while we were preparing the first draft of our manuscript. They use the same idea as in Proposition 2.1 to generate a posterior sample from a Gaussian process model. However, they fail to investigate when and how CG delivers practical computational gains. Our work is distinguished by the development — supported by both theoretical analysis and systematic empirical evaluations — of a novel preconditioning technique tailored toward sparse Bayesian regression problems (Section 2.4 and 2.5). In the process, we also compile a summary of the most practically useful linear algebra results scattered across the literature (Appendix B), facilitating potential applications of CG to a broader range of statistical problems.

The CG method solves a linear system $\Phi\beta = \mathbf{b}$ involving a positive definite matrix Φ as follows. Given an initial guess β_0 , which may be taken as $\beta_0 = \mathbf{0}$ for example, CG generates a sequence $\{\beta_k\}_{k=1,2,\dots}$ of increasingly accurate approximations to the solution. The convergence of the CG iterates β_k 's is intimately tied to the *Krylov subspace*

$$\mathcal{K}(\Phi, \mathbf{r}_0, k) = \text{span} \left\{ \mathbf{r}_0, \Phi\mathbf{r}_0, \dots, \Phi^{k-1}\mathbf{r}_0 \right\}, \quad (2.6)$$

generated from the initial residual $\mathbf{r}_0 = \Phi\beta_0 - \mathbf{b}$. With $\beta_0 + \mathcal{K}(\Phi, \mathbf{r}_0, k)$ denoting an affine space $\{\beta_0 + \mathbf{v} : \mathbf{v} \in \mathcal{K}(\Phi, \mathbf{r}_0, k)\}$, the approximate solution β_k satisfies the following optimality property in terms of a weighted l^2 norm:

$$\beta_k = \operatorname{argmin} \left\{ \|\beta' - \beta\|_{\Phi} : \beta' \in \beta_0 + \mathcal{K}(\Phi, \mathbf{r}_0, k) \right\} \quad \text{where } \|\mathbf{r}\|_{\Phi}^2 := \mathbf{r}^{\top}\Phi\mathbf{r}. \quad (2.7)$$

The norm $\|\cdot\|_{\Phi}$ is often referred to as the Φ -norm. The optimality property (2.7) in particular implies that CG yields the exact solution after p iterations. The main computational cost of each update $\beta_k \rightarrow \beta_{k+1}$ is a matrix-vector operation $\mathbf{v} \rightarrow \Phi\mathbf{v}$. Consequently, the required number of arithmetic operations to run p iterations of the CG update is comparable to that of a direct linear algebra method. For a typical precision matrix Φ arising from the conditional distribution (1.3), however, we can induce rapid convergence of CG through the preconditioning strategy described in the next section. In our numerical results, we indeed find that the distribution of β_k even for $k \ll p$ is indistinguishable from (1.3) for all practical purposes (Section 4.5).

2.3. Convergence theory of CG and its relation to the eigenvalue distribution

The iterative solution $\{\beta_k\}_{k=0,1,2,\dots}$ often displays slow convergence when CG is directly applied to a given linear system. Section 2.4 covers the topic of how to induce more rapid CG convergence for the system (2.5). In preparation, here we describe how the convergence behavior of CG is related to the structure of the positive definite matrix Φ .

CG convergence behavior is partially explained by the following well-known error bound given in terms of the *condition number* $\kappa(\Phi)$, the ratio of the largest to the smallest eigenvalue of Φ .

THEOREM 2.2. *Given a positive definite system $\Phi\beta = \mathbf{b}$ and a starting vector β_0 , the k -th CG iterate β_k satisfies the following bound in its Φ -norm distance to the solution β :*

$$\frac{\|\beta_k - \beta\|_{\Phi}}{\|\beta_0 - \beta\|_{\Phi}} \leq 2 \left(\frac{\sqrt{\kappa(\Phi)} - 1}{\sqrt{\kappa(\Phi)} + 1} \right)^k. \quad (2.8)$$

See Trefethen and Bau (1997) for a proof. Theorem 2.2 guarantees fast convergence of the CG iterates when the condition number $\kappa(\Phi)$ is small. On the other hand, a large condition number does not always prevent rapid convergence. This is because CG converges quickly also when the eigenvalues of Φ are “clustered.” The following theorem quantifies this phenomenon, albeit in an idealized situation in which Φ has exactly $k < p$ distinct eigenvalues.

THEOREM 2.3. *If the positive definite matrix Φ has only $k + 1$ distinct eigenvalues, then CG yields an exact solution within $k + 1$ iterations. In particular, the result holds if Φ is a rank- k perturbation of an identity i.e. $\Phi = \mathbf{F}\mathbf{F}^T + \mathbf{I}$ for $\mathbf{F} \in \mathbb{R}^{p \times k}$.*

See Golub and Van Loan (2012) for a proof.

Theorem 2.2 and 2.3 are arguably the two most famous results on the convergence property of CG, perhaps because their conclusions are clear-cut and easy to understand. These results, however, fall short of capturing the most important aspects of CG convergence behavior in practice. To address this problem, we bring together the most useful of the known results that have been scattered around the numerical linear algebra literature and summarize them as the following rule of thumb. All the statements below are made mathematically precise in Appendix B.

RULE OF THUMB 2.4. *Suppose that the eigenvalues $\nu_p(\Phi) \leq \dots \leq \nu_1(\Phi)$ of Φ are clustered in the interval $[\nu_{p-s}, \nu_r]$ except for a small fraction of them. Then CG effectively “removes” the outlying eigenvalues exponentially quickly. Its convergence rate subsequently accelerates as if the condition number in Eq 2.8 is replaced by the effective value ν_r/ν_{p-s} . The r largest eigenvalues are removed within r iterations, while the same number of smallest eigenvalues tends to delay convergence longer.*

2.4. Preconditioning the linear system (2.5) to accelerate CG convergence

A preconditioner is a positive definite matrix \mathbf{M} such that the preconditioned system

$$\tilde{\Phi}\tilde{\beta} = \tilde{\mathbf{b}} \quad \text{for } \tilde{\Phi} = \mathbf{M}^{-1/2}\Phi\mathbf{M}^{-1/2} \text{ and } \tilde{\mathbf{b}} = \mathbf{M}^{-1/2}\mathbf{b} \quad (2.9)$$

leads to faster convergence of the CG iterations. In practice, we only need \mathbf{M}^{-1} and not $\mathbf{M}^{-1/2}$ since the algorithm can be implemented so that only the operation $\mathbf{v} \rightarrow \mathbf{M}^{-1}\mathbf{v}$ is required to solve the preconditioned system (2.9) via CG (Golub and Van Loan, 2012). This preconditioned CG algorithm still returns a solution $\beta_k = \mathbf{M}^{-1/2}\tilde{\beta}_k$ in terms of the original system. While a wide range of general techniques has been proposed, finding a good preconditioner to a given linear system remains “a combination of art and science” (Saad, 2003).

In light of Rule of Thumb 2.4, an effective preconditioner should modify the eigenvalue structure of Φ so that the preconditioned matrix $\tilde{\Phi}$ has more tightly clustered eigenvalues except for a small number of outlying ones. Larger outlying eigenvalues are preferable over smaller ones, as smaller ones cause a more significant delay in CG convergence. Additionally, a choice of a preconditioner must take into consideration 1) the one-time cost of computing the preconditioner M itself and 2) the cost of operation $\mathbf{v} \rightarrow M^{-1}\mathbf{v}$ during each CG iteration.

In the contexts of sparse Bayesian regression, the linear system (2.5) turns out to admit a deceptively simple yet highly effective preconditioner. In fact, the choice

$$M = \tau^{-2}\Lambda^{-2} \quad (2.10)$$

yields a modified system (2.9) with an eigenvalue structure ideally suited to CG. With a slight abuse of terminology, we call it the *prior preconditioner* since it corresponds to the precision of $\beta | \tau, \lambda, \omega$ ($\stackrel{d}{=} \beta | \tau, \lambda$) before observing \mathbf{y} and \mathbf{X} . Most existing preconditioners require explicit access to the elements of Φ for their constructions (Golub and Van Loan, 2012) and are thus useless when computing Φ itself is a bottleneck. The Jacobi preconditioner $M = \text{diag}(\Phi_{11}, \dots, \Phi_{pp})$ is arguably the only reasonable alternative and is known to be one of the most effective when the matrix is diagonally-dominant as in our case. However, our numerical results clearly show superior performances of the prior preconditioner (Section 3.3 and 4.4).

A heuristic motivation behind the prior-preconditioner is as follows. When employing the shrinkage prior, we expect posterior draws of $\tau\lambda$ to satisfy $\tau\lambda_j \approx 0$ except for a relatively small subset $\{j_1, \dots, j_k\}$ of $j = 1, \dots, p$. (More precisely, we mean by $\tau\lambda_j \approx 0$ that the contribution of the term $x_{ij}\beta_j | \tau, \lambda_j$ is small in predicting the outcome.) We now note that the prior-preconditioned matrix is given by

$$\tilde{\Phi} = \tau^2\Lambda\mathbf{X}^\top\Omega\mathbf{X}\Lambda + \mathbf{I}_p, \quad (2.11)$$

and the matrix $\tau^2\Lambda\mathbf{X}^\top\Omega\mathbf{X}\Lambda$ has the (i, j) -th entry

$$(\tau^2\Lambda\mathbf{X}^\top\Omega\mathbf{X}\Lambda)_{i,j} = (\tau\lambda_i)(\tau\lambda_j) (\mathbf{X}^\top\Omega\mathbf{X})_{ij}, \quad (2.12)$$

which is small when either $\tau\lambda_i \approx 0$ or $\tau\lambda_j \approx 0$. In other words, the entries of $\tau^2\Lambda\mathbf{X}^\top\Omega\mathbf{X}\Lambda$ are small away from the $k \times k$ block corresponding to the indices $\{j_1, \dots, j_k\}$. In general, smaller entries of a matrix have less contributions to the eigenvalue structures of the entire matrix (Golub and Van Loan, 2012). This means that the prior-preconditioned matrix (2.11) can be thought of as a perturbation of the identity with a matrix with approximate low-rank structure.† As such, $\tilde{\Phi}$ can be expected to have eigenvalues clustered around 1, except for a relatively small number of larger ones. Supplement Section S1 provides an alternative motivation of the prior preconditioner based on the expected behavior of a posterior under a strongly informative prior.

†It is too naive, however, to conclude that we obtain a good approximation to $\tilde{\Phi}$ by simply zeroing out $\tau\lambda_j$'s below some threshold. While such thresholding approach is successfully employed in Johndrow et al. (2018) for a related but different problem, our numerical results clearly show that such approximation can be of a poor quality (Supplement Section S6).

2.5. Theory of prior-preconditioning and the role of sparsity in a posterior

We now formally quantify the eigenvalue structure of the matrix (2.11).

THEOREM 2.5. *Let $\lambda_{(k)} = \lambda_{j_k}$ denote the k -th largest element of $\{\lambda_1, \dots, \lambda_p\}$. The eigenvalues of the prior-preconditioned matrix (2.11) then satisfies*

$$1 \leq \nu_k(\tilde{\Phi}) \leq 1 + \tau^2 \lambda_{(k)}^2 \nu_1(\mathbf{X}^\top \Omega \mathbf{X}) \quad (2.13)$$

for $k = 1, \dots, p$. In fact, the following more general bounds hold. Let $\mathbf{A}_{(-k)}$ denote the $(p-k) \times (p-k)$ submatrix of a given matrix \mathbf{A} corresponding to the row and column indices j_{k+1}, \dots, j_p . With this notation, we have

$$1 \leq \nu_{k+\ell}(\tilde{\Phi}) \leq 1 + \tau^2 \lambda_{(k)}^2 \nu_{\ell+1}((\mathbf{X}^\top \Omega \mathbf{X})_{(-k)}) \leq 1 + \tau^2 \lambda_{(k)}^2 \nu_{\ell+1}(\mathbf{X}^\top \Omega \mathbf{X}) \quad (2.14)$$

for any $k \geq 1$ and $\ell \geq 0$ such that $1 \leq k + \ell \leq p$.

Theorem 2.5 guarantees tight clustering of the eigenvalues of the prior-preconditioned matrix — and hence rapid convergence of CG — when most of $\tau \lambda_j$'s are close to zero. Through its dependence on $\nu_\ell(\mathbf{X}^\top \Omega \mathbf{X})$, the bound (2.14) further indicates rapid CG convergence when the eigenvalues of $\mathbf{X}^\top \Omega \mathbf{X}$ decays quickly (for example due to high-collinearity among the predictors). We can also directly relate the prior-preconditioned CG approximation error to the decay rate in $\tau \lambda_{(k)}$'s:

THEOREM 2.6. *The prior-preconditioned CG applied to (2.5) yields iterates satisfying the following bound for any $m, m' \geq 0$:*

$$\frac{\|\beta_{m+m'} - \beta\|_{\Phi}}{\|\beta_0 - \beta\|_{\Phi}} \leq 2 \left(\frac{\tilde{\kappa}_m^{1/2} - 1}{\tilde{\kappa}_m^{1/2} + 1} \right)^{m'} \quad (2.15)$$

where $\tilde{\kappa}_m = 1 + \min_{k+\ell=m} \tau^2 \lambda_{(k+1)}^2 \nu_{\ell+1}((\mathbf{X}^\top \Omega \mathbf{X})_{(-k)})$.

See Appendix A for proofs of Theorem 2.5 and 2.6.

To illustrate the implication of Theorem 2.6 in concrete terms, suppose that a posterior draw $\tau, \boldsymbol{\lambda}, \boldsymbol{\omega}$ satisfies $\tau^2 \lambda_{(m+1)}^2 \nu_1(\mathbf{X}^\top \Omega \mathbf{X}) \leq 100$ for some m . In this case, we have $\log_{10}(\tilde{\kappa}_m^{1/2} - 1)/(\tilde{\kappa}_m^{1/2} + 1) \leq -0.086$. So the bound (2.15) implies

$$\frac{\|\beta_{m+m'} - \beta\|_{\Phi}}{\|\beta_0 - \beta\|_{\Phi}} \leq 2 \cdot 10^{-0.086m'}. \quad (2.16)$$

After $m + 100$ iterations, the CG approximation error in the Φ -norm is guaranteed to be reduced by a factor of $2 \cdot 10^{-8.6} \approx 10^{-8.3}$ relative to the initial error.

While we have so far stated the theoretical results in linear algebraic languages, the purpose of the prior-preconditioner is efficient posterior computation under sparse regression models. We now summarize our discussions in a more statistical language to provide a practical guideline on the CG sampler performance.

RULE OF THUMB 2.7. *The prior-preconditioned CG applied to the linear system (2.5) converges rapidly when the posterior of β concentrates on sparse vectors with most of β_j 's virtually negligible in magnitudes. As the sparsity of β increases, the convergence rate of the CG sampler also increases.*

The statements above are born out by illustrative examples of Section 3 using synthetic sparse regression posteriors. As we have seen, the statements can be made more precise in terms of the decay rate in the ordered statistics $\tau\lambda_{(k)}$ of a posterior sample $\tau\lambda$ (Rule of Thumb 2.4, Theorem 2.5, and Theorem 2.6).

2.6. Practical details on deploying the CG sampler for sparse regression

While prior preconditioning is undoubtedly the most essential ingredient, there remain a few more important details in applying the CG sampler to sparse regression posterior computation. These are 1) a choice of the initial CG vector β_0 , 2) a termination criteria for CG, and 3) handling of regression coefficients with uninformative priors. We discuss them briefly here and defer more thorough discussions to Supplement Section S2.

A choice of the initial vector has little effect on the eventual exponential convergence rate of CG and, while not to be neglected, is nowhere as consequential as that of the preconditioner (Meurant, 2006). In fact, we find that any reasonable choice works fine in our numerical results (Section S2.1). In its typical applications, CG is terminated when the ℓ^2 -norm of the residual $\mathbf{r}_k = \Phi\beta_k - \mathbf{b}$ falls below some prespecified threshold. Utility of $\|\mathbf{r}_k\|$ as an error metric is dubious for the purpose of the CG sampler, however. We instead propose the prior-preconditioned residual $\tilde{\mathbf{r}}_k = \tilde{\Phi}\tilde{\beta}_k - \tilde{\mathbf{b}}$ as an alternative, more tailored and interpretable for our purpose (Section S2.2). When preconditioning CG, regression coefficients with uninformative priors, such as the intercept, must be handled differently from those under shrinkage. We can accommodate such coefficients by augmenting the prior-preconditioner with another diagonal matrix. We analyze the eigenvalues of the resulting preconditioned matrix and show that the convergence rate remains fast and is robust to the precise choice of the diagonal matrix (Section S2.3).

3. Simulation study of the CG sampler performance on synthetic posteriors

We study the CG sampler performance when applied to actual posterior conditional distributions of the form (1.3). We simulate data with varying numbers of non-zero coefficients and confirm how sparsity in regression coefficients translates into faster CG convergence as predicted by Theorem 2.5 and Rule of Thumb 2.7. We also illustrate how the convergence rates are affected by different preconditioning strategies and by corresponding eigenvalue distributions of the preconditioned matrices.

3.1. Choice of shrinkage prior: Bayesian bridge

Among the existing global-local shrinkage priors of the form (1.1), in this article we adopt the Bayesian bridge prior of Polson et al. (2014) for the following reasons. First, the Gibbs sampler under the Bayesian bridge tends to demonstrate better mixing in the global shrinkage parameter τ . This is because the Bayesian bridge formulation allows the update of τ from the distribution of $\tau | \beta, \omega, \mathbf{y}, \mathbf{X}$ with λ marginalized out (Polson et al., 2014). Secondly, many of the alternative shrinkage priors have extremely heavy tails that can be problematic under the logistic model.

When the regression coefficients are only weakly identified from the data, the posterior may turn out also heavy-tailed, causing issues in terms of both computation and inference (Ghosh et al., 2018; Piironen and Vehtari, 2017).

Under the Bayesian bridge, the local shrinkage parameter λ_j 's are given independent alpha-stable distributions with index of stability $\alpha/2$ with $0 < \alpha \leq 1$. The corresponding prior on $\beta_j | \tau$, when λ_j is marginalized out, is

$$\pi(\beta_j | \tau) \propto \tau^{-1} \exp(-|\beta_j/\tau|^\alpha). \quad (3.17)$$

The case $\alpha = 1$ coincides with the Bayesian lasso. The distribution of $\beta_j | \tau$ becomes “spikier” as $\alpha \rightarrow 0$, placing greater mass around 0 while at the same time having heavier tails. While an alpha-stable distribution has no closed-form expression, there are algorithms available to efficiently sample from the posterior distribution of $\lambda_j | \beta_j, \tau$ (Polson et al., 2014). In typical applications, the marginal likelihood of data favors the values $\alpha < 1$ but identifies α only very weakly (Polson et al., 2014), so in this article we simply fix $\alpha = 1/2$.

3.2. Experimental set-up

We generate synthetic data of sample size $n = 25,000$ with the number of predictors $p = 10,000$. In constructing a design matrix \mathbf{X} , we emulate a model from factor analysis (Jolliffe, 2002). We first sample a set of $m = 99$ orthonormal vectors $\mathbf{u}_1, \dots, \mathbf{u}_m \in \mathbb{R}^p$ uniformly from a Stiefel manifold. We then set the predictor \mathbf{x}_i for the i -th observation to be

$$\mathbf{x}_i = \sum_{\ell=1}^{99} f_{i,\ell} \mathbf{u}_\ell + \boldsymbol{\epsilon}_i \quad \text{for } f_{i,\ell} \sim \mathcal{N}(0, (100 - \ell)^2) \text{ and } \boldsymbol{\epsilon}_i \sim \mathcal{N}(\mathbf{0}, \mathbf{I}_p). \quad (3.18)$$

This is equivalent to sampling $\mathbf{x}_i \sim \mathcal{N}(\mathbf{0}, \mathbf{U} \mathbf{D} \mathbf{U}^\top)$, where \mathbf{D} is a diagonal matrix with $\sqrt{D_{\ell\ell}} = \max\{100 - \ell, 1\}$ and \mathbf{U} is an orthonormal matrix sampled uniformly from the space of orthonormal matrices. We then center and standardize the predictors as is commonly done before applying sparse regression (Hastie et al., 2009).

The above process yields a design matrix \mathbf{X} with moderate correlations among the p predictors — the distribution of pairwise correlations is approximately Gaussian centered around 0 with the standard deviation of 0.13. Based on this design matrix \mathbf{X} , we simulate three different binary outcome vectors by varying the number of non-zero regression coefficients. More specifically, we consider a sparse regression coefficient $\boldsymbol{\beta}_{\text{true}}$ with $\beta_{\text{true},j} = \mathbf{1}\{j \leq K\}$ with varying numbers of signals $K = 10, 20$, and 50. In all three scenarios, the binary outcome y_i 's are generated from the logistic model as $y_i | \boldsymbol{\beta}_{\text{true}}, \mathbf{x}_i \sim \text{Bernoulli}(p_i)$ for $\text{logit}(p_i) = \mathbf{x}_i^\top \boldsymbol{\beta}_{\text{true}}$.

For each simulated data set, we obtain a posterior sample of $\boldsymbol{\omega}, \tau, \boldsymbol{\lambda} | \mathbf{y}, \mathbf{X}$ by running the Polya-Gamma augmented Gibbs sampler with the brute-force direct linear algebra to sample $\boldsymbol{\beta}$ from its conditional distribution (1.3). We confirm the convergence of the Markov chain by examining the traceplot of the posterior log density of $\boldsymbol{\beta}, \tau | \mathbf{y}, \mathbf{X}$ (with $\boldsymbol{\lambda}$ and $\boldsymbol{\omega}$ marginalized out). Having obtained a posterior sample $\boldsymbol{\omega}, \tau, \boldsymbol{\lambda}$, we sample a vector \mathbf{b} as in (2.4) and apply CG to the linear system

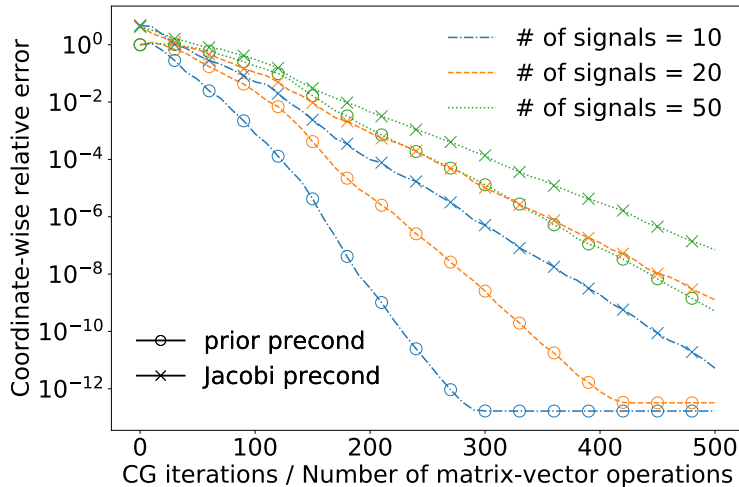


Fig. 3.1. Plot of the CG approximation error v.s. the number of CG iterations. The CG sampler is applied to synthetic sparse regression posteriors. The different line styles correspond to the different numbers of true signals. The circle and cross markers denote the uses of the prior and Jacobi preconditioners.

(2.5). We then compare the CG iterates $\{\beta_k\}_{k>0}$ to the exact solution β_{direct} obtained by solving the same system with the Cholesky-based direct method. We repeat this process for 8 random replications of the right-hand vector \mathbf{b} .

3.3. Results: convergence rates, eigenvalues, and sparsity of coefficients

Figure 3.1 shows the CG approximation error as a function of the number of CG iterations, whose cost as we discuss in Section 2.2 is dominated by matrix-vector multiplications $\mathbf{v} \rightarrow \Phi \mathbf{v}$. We characterize the approximation error as the relative error $|(\beta_k - \beta_{\text{direct}})_j / (\beta_{\text{direct}})_j|$ averaged across all the coefficients. Each line on the plot shows the geometric average of this error metric over the random replications of \mathbf{b} . In Supplement Section S3, we show that the CG convergence behavior observed here remains qualitatively similar regardless of choice of the error metric and varies little across the different right-hand vectors.

We first focus on the approximation errors under the prior preconditioner, indicated by the lines with circles. After $k \ll p = 10,000$ matrix-vector operations, the distance between β_k and β_{direct} is already orders of magnitudes smaller than typical Monte Carlo errors. In fact, with some additional CG iterations, the distance reaches the level of machine precision; notice the eventual “plateaus” achieved under the prior preconditioner in the $K = 10$ and $K = 20$ cases.

Figure 3.1 also shows the approximation errors under the Jacobi preconditioner $\mathbf{M} = \text{diag}(\Phi_{11}, \dots, \Phi_{pp})$. As discussed in Section 2.4, when using the CG sampler for the applications considered in this article, the Jacobi preconditioner is the only reasonable alternative among the existing general-purpose ones. The prior preconditioner is clearly superior, with the difference in convergence speed more pronounced

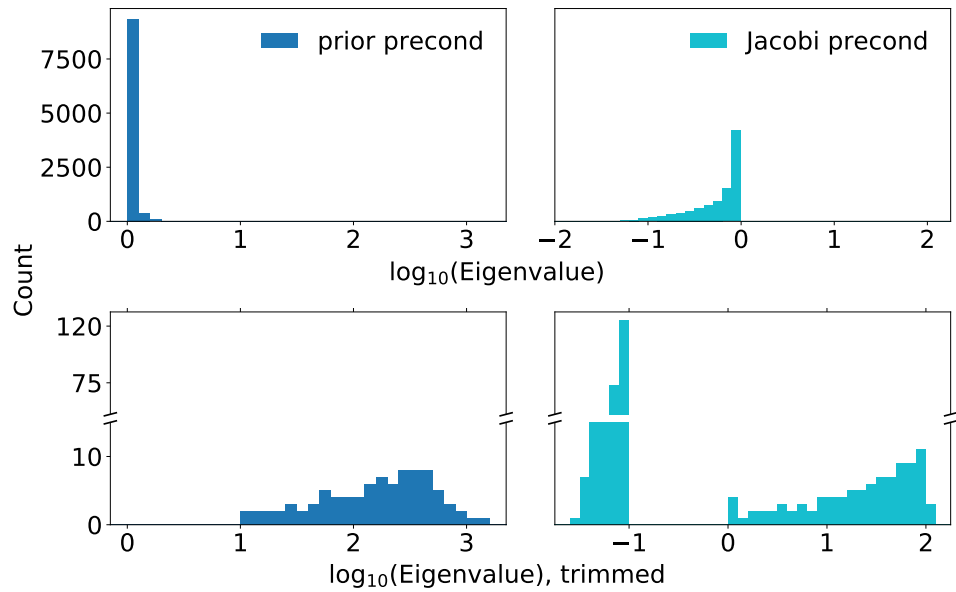
when true regression coefficients are sparser. Studying the eigenvalue distributions of the respective preconditioned matrices provides further insight into the observed convergence behaviors. Figure 3.2 (a) & (b) show the eigenvalue distributions of the preconditioned matrices based on a posterior sample from the synthetic data with $K = 10$. The trimmed version of the histograms are also given to highlight the tails of the distributions. The prior preconditioner induces the distribution with a tight cluster around 1 (or 0 in the \log_{10} scale) with a relatively small number of large ones, confirming the theory developed in Section 2.5. On the other hand, the Jacobi preconditioner induces a more spread-out distribution, problematically introducing quite a few small eigenvalues that delay the CG convergence (Rule of Thumb 2.4).

Finally, we turn our attention to the relationship as seen in Figure 3.1 between the CG convergence rate and the sparsity in the underlying true regression coefficients. The convergence is clearly quicker when the true regression coefficients are sparser. To understand this relationship, it is informative to look at the values of $\tau\lambda_j = \mathbb{E}[\beta_j | \tau, \boldsymbol{\lambda}]$ drawn from the respective posterior distributions. Figure 3.3 plots the values of $\tau\lambda_j$ for $j = 1, \dots, 250$ corresponding to the first 250 coefficients. We use two different y -scales for $K = 10$ and $K = 50$, shown on the left and right respectively, to facilitate qualitative comparison between the two cases. As expected, the posterior sample from the synthetic data with a larger number of signals has a larger number of $\tau\lambda_j$'s away from zero. These relatively large $\tau\lambda_j$'s contribute to the delayed convergence of CG (Theorem 2.5 and Rule of Thumb 2.4).

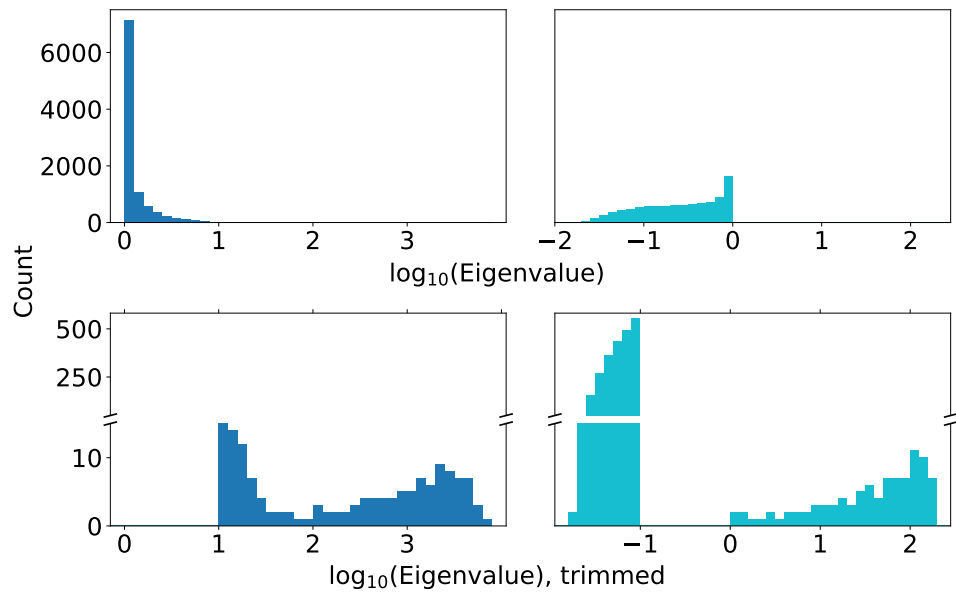
A more significant cause of the delay, however, is the fact that the shrinkage prior yields weaker shrinkage on the zero coefficients when there are a larger number of signals. With a close look at Figure 3.3, one can see that $\tau\lambda_1, \dots, \tau\lambda_K$ corresponding to the true signals are not as well separated from the rest of $\tau\lambda_j$'s when $K = 50$. In fact, the histograms on the left of Figure 3.4 shows that the distribution of $\tau\lambda_j$'s for $K = 50$ are shifted toward larger values compared to that for $K = 10$. This is mostly due to the posterior distribution of τ concentrating around a larger value — the value of the posterior sample is $\tau \approx 2.0 \times 10^{-3}$ for the $K = 10$ case while $\tau \approx 6.7 \times 10^{-3}$ for the $K = 50$ case. It is also worth taking a closer look at the tail of the distribution of $\tau\lambda_j$'s. The histograms on the right of Figure 3.4 show the distribution of the 250 largest $\tau\lambda_j$'s after scaling them by $\max_j \tau\lambda_j$. The figure makes it clear that $\tau\lambda_j$'s corresponding to the true signals are much more well separated from the rest when $K = 10$. Overall, the slower decay in the largest values of $\tau\lambda_j$'s results in the eigenvalues of the preconditioned matrices having a less tight cluster around 1; compare the eigenvalue distributions of Figure 3.2.(a) & (b) to those of Figure 3.2.(c) & (d).

4. Application: comparison of two drugs using healthcare databases

In this section, we demonstrate how CG-acceleration delivers an order of magnitude speed-up in the posterior computation for a large-scale observational study. We apply sparse Bayesian logistic regression to conduct a comparative study of two blood anti-coagulants *dabigatran* and *warfarin*. The goal of the study is to quantify which of the two drugs have a lower risk of intracranial hemorrhage (bleeding inside



(a) Based on synthetic data with 10 non-zero coefficients.



(b) Based on synthetic data with 50 non-zero coefficients.

Fig. 3.2. Histograms of the eigenvalues of the preconditioned matrices. The eigenvalues under the prior preconditioner are shown on the left and those under the Jacobi on the right. Shown on the lower row are the trimmed versions of the histograms, in which we remove the eigenvalues in the range $[0, 1]$ in the \log_{10} scale for the prior preconditioner and those in the range $[-1, 0]$ for the Jacobi. The y -axes for the trimmed histograms have intermediate values removed to make small counts more visible. The width of the bins are kept constant throughout so that the y -axis values of the bars are proportional to probability densities and thus can be compared meaningfully across the plots.

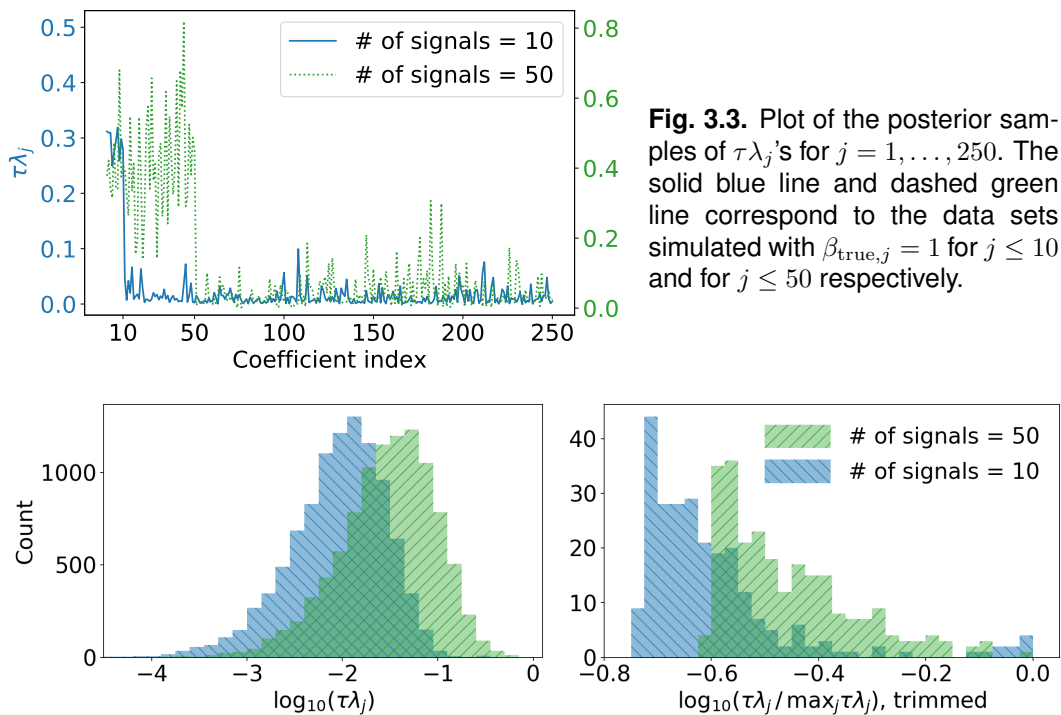


Fig. 3.3. Plot of the posterior samples of $\tau\lambda_j$'s for $j = 1, \dots, 250$. The solid blue line and dashed green line correspond to the data sets simulated with $\beta_{\text{true},j} = 1$ for $j \leq 10$ and for $j \leq 50$ respectively.

Fig. 3.4. Histograms of the posterior samples of $\tau\lambda_j$'s. The histograms with two different colors correspond to the distinct posteriors with 10 and 50 non-zero regression coefficients. The histograms on the right better expose the relative tail behaviors in the two distributions of $\tau\lambda_j$'s by taking only the 250 largest values and plotting their magnitude relative to $\max_j \tau\lambda_j$.

the skull). This question has previously been investigated by Graham et al. (2015) and our analysis yields clinical findings consistent with theirs (Section 4.6).

We are particularly interested in sparse Bayesian regression as a tool for the Observational Health Data Sciences and Informatics (OHDSI) collaborative (Hripcsak et al., 2015). Hence, we follow the OHDSI protocol in pre-processing of the data as well as in estimating the treatment effect. In particular, sparse regression plays a critical role in eliminating hand-picking of confounding factors; this enables the application of a reproducible and consistent statistical estimation procedure to tens of thousands of observational studies (Schuemie et al., 2018b,a; Tian et al., 2018).

4.1. Data set

We extract patient-level data from Truven Health MarketScan Medicare Supplemental and Coordination of Benefits Database. In the database, we find $n = 72,489$ patients who became first-time users of either dabigatran or warfarin after diagnosis of atrial fibrillation. Among them, 19,768 are treated with dabigatran and the rest with warfarin. There are $p = 98,118$ predictors, consisting of clinical measurements, pre-existing conditions, as well as prior treatments and administered drugs — all

measured before exposure to dabigatran or warfarin. Following the OHDSI protocol, we screen out the predictors observed in less than 0.1% of the cohort. This reduces the number of predictors to $p = 22,175$. The precise definition of the cohort can be found at <http://www.ohdsi.org/web/atlas/#/cohortdefinition/{2978,2979,2981}>.

Each patient has or is exposed to only a small subsets of the potential pre-existing conditions, treatments, and drugs. The design matrix \mathbf{X} therefore is sparse, with only 4% of the entries being non-zero. Another noteworthy feature of the data is the low incidence rates of intracranial hemorrhage; the outcome indicator \mathbf{y} has non-zero entries $y_i = 1$ for only 192 out of 72,489 patients.

4.2. Statistical approach: propensity score method for treatment effect estimation

To control for covariate imbalances between the dabigatran and warfarin users in estimating the average treatment effect, we use a doubly-robust method with propensity score stratification. The procedure involves two logistic models with large numbers of predictors, to deal with which we employ sparse Bayesian regression. We describe the procedure and essential ideas below but refer the readers to Stuart (2010) and the references therein for further details.

Estimation of the treatment effect proceeds in two stages. First, the *propensity score* $\mathbb{P}(T_i = 1 | \mathbf{x}_i)$ of the treatment assignment to dabigatran is estimated by the logistic model

$$\text{logit}\{\mathbb{P}(T_i = 1 | \mathbf{x}_i)\} = \beta_0 + \mathbf{x}_i^\top \boldsymbol{\beta}. \quad (4.19)$$

The quantiles of the estimated propensity scores are then used to stratify the population into subgroups of equal sizes. Following a typical recommendation, we choose the number of subgroups as $M = 5$. Under suitable assumptions, conditioning on the strata indicator removes most of imbalances in the distributions of the predictors between the treatment ($T_i = 1$) and control ($T_i = 0$) groups.

After the propensity score stratification, we estimate the average treatment effect α_0 via the logistic model

$$\text{logit}\{\mathbb{P}(y_i = 1 | \boldsymbol{\alpha}, \boldsymbol{\beta}, s_i, \mathbf{x}_i)\} = \beta_0 + \alpha_0 T_i + \sum_{m=2}^M \alpha_m \mathbf{1}\{s_i = m\} + \mathbf{x}_i^\top \boldsymbol{\beta}, \quad (4.20)$$

where a categorical variable s_i denotes the strata membership of the i -th individual. (With a slight abuse of notation, we use $\boldsymbol{\beta}$ in both of the models (4.19) and (4.20) to denote the regression coefficients of predictors.) The indicator of $s_i = 1$ is excluded from the model for identifiability. The inclusion of the predictor \mathbf{x}_i is not necessary if conditioning on the strata s_i achieves perfect covariate balance. Controlling for the predictor \mathbf{x}_i , however, makes the treatment estimation procedure more robust to potential misspecification in the propensity score model (4.19) as well as to any covariate imbalances that remain after conditioning on s_i .

4.3. Prior choice and posterior computation

We fit the models (4.19) and (4.20) using the Bayesian bridge shrinkage prior (see Section 3.1) on the regression coefficients. A reference prior $\pi(\tau) \propto 1/\tau$ is used

for the global shrinkage parameter (Berger et al., 2009) and an uninformative prior $\pi(\beta_0) \propto 1$ for the intercept. For the average treatment effect and propensity score strata effects, we place weakly informative $\mathcal{N}(0, 1)$ priors.

For posterior computation, we compare two Gibbs samplers that differ only in their methods for the conditional updates of β from the distribution (1.3). One of the samplers uses the proposed CG sampler, while the other uses a traditional direct method based on the Cholesky factorization. (Sparse Cholesky methods offer no computational speed-up here as the precision matrix, despite the sparsity in the design matrix \mathbf{X} , is almost completely dense; see Supplement Section S4.) We refer to the respective sampler as the *CG-accelerated* and *direct* Gibbs sampler. The other conditional updates follow the approaches described in Polson et al. (2014).

We implement the Gibbs samplers in Python and run on 2015 iMac with Intel Core i7 processors. For all the linear algebra operations, we interface our Python code with the Intel Math Kernel Library (MKL) implementations of Basic Linear Algebra Subprograms (BLAS) and sparse BLAS, which proved computationally superior to alternatives in our preliminary benchmarking. Details on how we optimized both Gibbs sampler are described in Supplement Section S4.

4.4. Overall speed-up from CG acceleration and posterior characteristics

We run the Markov chains for 1,500 and 2,000 iterations for the propensity score and treatment effect model respectively, yielding 1,000 post-convergence samples. For both Gibbs samplers, the total computation times are dominated by the conditional updates of β from (1.3). The magnitudes of CG-acceleration therefore are determined by the convergence rates of the CG sampler at each Gibbs iteration. The direct Gibbs sampler requires 50.3 hours for the propensity score model and 69.5 hours for the treatment effect model. On the other hand, the CG-accelerated sampler finishes in 5.24 and 3.25 hours, yielding **9.6-fold** and **21-fold** speed-ups.

In agreement with the theory and results of Section 2.5 and 3.3, the variability in the magnitudes of CG-acceleration can be explained by the posterior sparsity structures of the regression coefficients. As a measure of sparsity, for each regression coefficient we consider two quantities: one-sided tail probability, the larger of the posterior probabilities of $\beta_j > 0$ or $\beta_j < 0$, and magnitude of the posterior mean.

For the propensity score model, 40 and 85 out of the 22,175 regression coefficients have one-sided tail probabilities above 97.5% and 90% respectively. Only 79 regression coefficients have the magnitudes of their posterior means above 0.1, while 18,161 (81.9%) of the coefficients have the magnitudes below 0.01. For the treatment effect model, some of the regression coefficients have bi-modal marginal posteriors and their samples occasionally deviate away from zero. Averaged over all the posterior draws, however, except for the fixed effects no regression coefficient comes out as significant. This suggests that the propensity score stratification is indeed successful in balancing the distribution of \mathbf{x}_i 's and it may have been unnecessary to include those predictors in the treatment effect model. Of course, we can only conclude this after actually fitting the doubly-robust model. As the Gibbs sampler requires close to 1,000 iterations before convergence, the burn-in iterations alone

would be a significant computational burden if it were not for the CG-acceleration.

For more in-depth analysis of the CG-acceleration mechanism, in Supplement Section S5 we examine the CG sampler behavior at each Gibbs iteration. In particular, we verify that the error metric discussed in Section 2.6 works well in deciding when to terminate the CG iteration. We also confirm that the advantage of the prior preconditioner over the Jacobi one continues to hold in this real data example.

4.5. Accuracy of the CG sampler

Since technically CG does not yield the exact solution when terminated at $k < p$ iterations, we assess the accuracy of the samples generated by the CG-accelerated Gibbs by comparing them against the “ground truth” samples generated by the direct Gibbs. As we show, perturbation of the target distribution due to the CG approximation error is, if any, so small that it is essentially negligible.

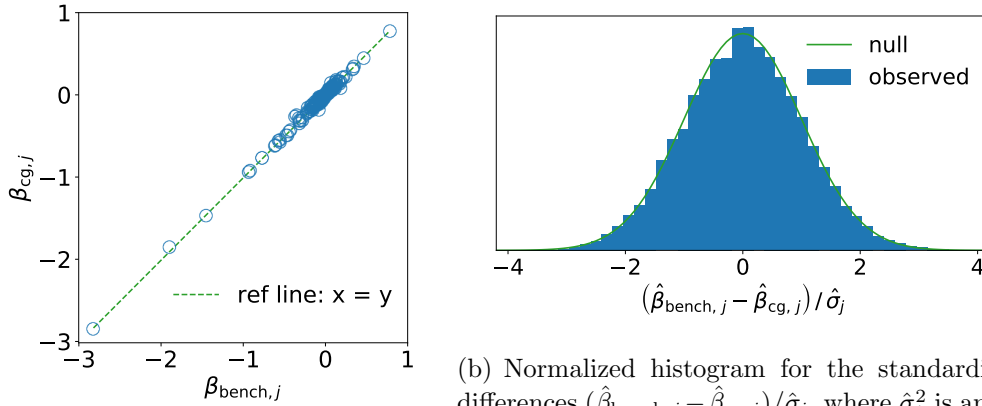
In comparing the two sets of samples, we encountered one complication. The global shrinkage parameter τ generally demonstrates good mixing under the Bayesian bridge prior (see Section 3.1); however, for our real world examples it proved difficult to obtain a sufficiently large effective sample size for τ within a reasonable amount of time. To ensure that the effective sample sizes for β are large enough to adequately characterize the stationary distribution, therefore, we employed an empirical Bayes approach. We first find a value $\hat{\tau}$ which approximately maximizes the marginal likelihood through Monte Carlo expectation-maximization algorithm (Park and Casella, 2008). We then run the two samplers conditional on $\tau = \hat{\tau}$.

We test for differences between the two sets of the MCMC samples as follows. We first set $\hat{\beta}_{\text{bench}}$ and $\hat{\beta}_{\text{cg}}$ to be the posterior means estimated by averaging the samples from the direct Gibbs (used as a benchmark) and CG-accelerated Gibbs. Figure 4.5(a) graphically compares these two estimators as an informal sanity check. We then estimate the effective sample sizes of β_j from the respective samplers using the R CODA package (Plummer et al., 2006). These estimated effective sample sizes can be used to estimate the Monte Carlo standard deviations $\hat{\sigma}_j$ of the differences $\hat{\beta}_{\text{bench},j} - \hat{\beta}_{\text{cg},j}$. When the two sets of samples have the same stationary distribution, the standardized differences $(\hat{\beta}_{\text{bench},j} - \hat{\beta}_{\text{cg},j})/\hat{\sigma}_j$ are approximately distributed as the standard Gaussians by the Markov chain central limit theorem (Geyer, 2011).

Figure 4.5(b) confirms that the distribution of the standardized differences closely follows the “null” distribution. Figure 4.5(a) and 4.5(b) are based on the posterior samples for the propensity score model, but we obtained essentially the same result under the treatment effect model. We additionally performed the same diagnostic on the estimators of the posterior second moment of β and obtained similar results.

4.6. Clinical conclusions from the dabigatran v.s. warfarin study

The propensity score model finds substantial differences between the patients treated by dabigatran and warfarin. In particular, patients’ covariate characteristics are predictive of the treatment assignments as seen in Figure 4.6. With the Bayesian approach, it is also straightforward to obtain uncertainty in the propensity score



(a) Comparison of the regression coefficient estimates (posterior means) between those based on the direct and CG-accelerated Gibbs samplers.

(b) Normalized histogram for the standardized differences $(\hat{\beta}_{\text{bench},j} - \hat{\beta}_{\text{cg},j}) / \hat{\sigma}_j$, where $\hat{\sigma}_i^2$ is an estimate of the Monte Carlo variance of $\hat{\beta}_{\text{bench},j} - \hat{\beta}_{\text{cg},j}$. Gaussianity of the histogram indicates no statistically significant difference between the two MCMC outputs.

Fig. 4.5. Diagnostic plots to check for any statistically significant differences in the two MCMC outputs.

estimates. For instance, we can easily characterize uncertainty in the *inverse probability weight*, defined as a function of the propensity score p_i as $w_i = p_i^{-1}$ if the i -th individual is in the treated group and $w_i = (1 - p_i)^{-1}$ if in the control group. Inverse probability weights are widely used due to their desirable theoretical properties, but have known issues of being unstable (Stuart, 2010). In fact, Figure 4.7 shows that the posterior uncertainties of the weights can be as large as their posterior means.

The two most significant predictors are the treatment year and age group. Both predictors have been encoded as binary indicators in the design matrix for simplicity, but the coefficients of categorical and ordinal predictors could have been estimated with shrinkage priors analogous to Bayesian grouped or fused lasso (Kyung et al., 2010; Xu et al., 2015). The posterior mean and 95% credible intervals of the regression coefficients are shown in Figure 4.8. The figure plots the effect sizes relative to the year 2010 and the age group 65 ~ 69; when actually fitting the model, however, we use the most common category as a baseline for categorical variables.

For the treatment effect model, Figure 4.9(a) shows the posterior distribution of the average treatment effect of dabigatran over warfarin. The posterior indicates an evidence, though not a conclusive one, for the lower incidence rate of intracranial hemorrhage under dabigatran treatment. This is consistent with findings of Graham et al. (2015). The violin plot of Figure 4.9(b) summarizes the posterior distributions of the baseline incident rates within each propensity score strata. While the differences in the baseline incident rates may seem insignificant from their marginals, the baseline for the 2nd quintile actually has more than 95% posterior probability of being larger than those for the 1st and 5th quintile.

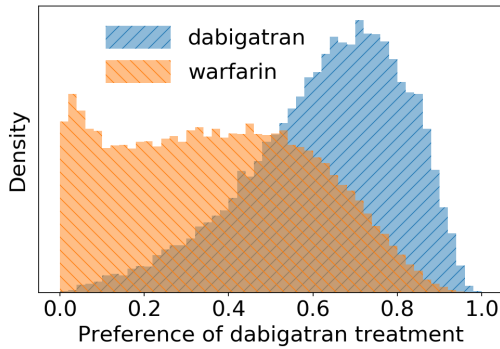


Fig. 4.6. Normalized histogram of the estimated preference scores for each group. Preference score transforms raw propensity score to make it a more interpretable measure (Walker et al., 2013).

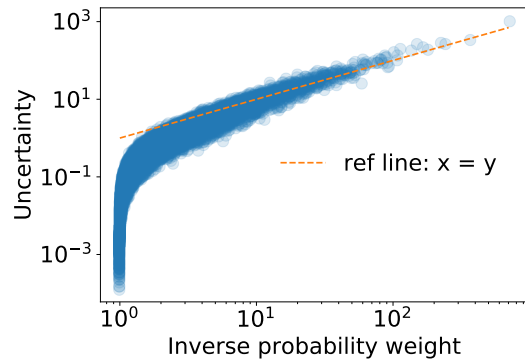


Fig. 4.7. Posterior means of the inverse probability weights, plotted against twice the posterior standard deviations used as measures of uncertainty. The axes are in the log-log scale and the dashed line indicates the coordinates $x = y$.

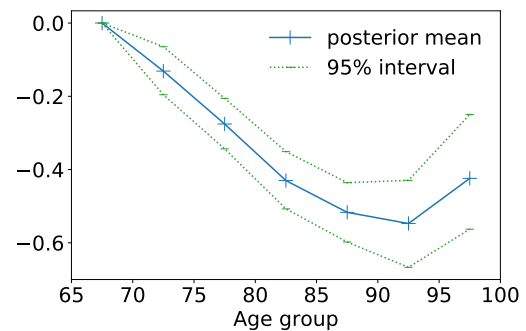
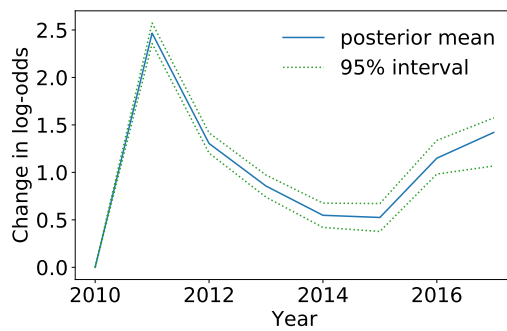
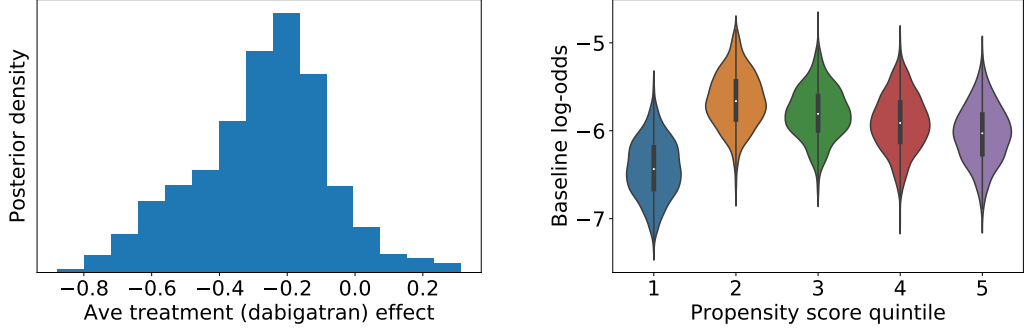


Fig. 4.8. Posterior means and 95% credible intervals for the regression coefficients of the treatment year and age group indicators. The age groups are divided into 5-year windows.

5. Acknowledgment

We thank Yuxi Tian and Martijn Schuemie for their help in wrangling the data set used in Section 4. We also thank Jianfeng Lu and Ilse Ipsen for useful discussions on linear algebra topics. This work is partially supported by National Science Foundation grant DMS 1264153 and National Institutes of Health grant U19 AI135995.



(a) Average effect of treatment by dabigatran over warfarin on the incident rates of intracranial hemorrhage. (b) Violin plot of the baseline incident rates of intracranial hemorrhage within each propensity score strata.

Fig. 4.9. Posterior distributions from the treatment effect model.

Appendix A Proofs

We first derive Theorem 2.6 as a consequence of Theorem 2.5 before we proceed to prove Theorem 2.5.

PROOF (THEOREM 2.6). By Theorem B.4, the $(m + m')$ -th CG iterate $\beta_{m+m'}$ satisfies the following bound:

$$\frac{\|\beta_{m+m'} - \beta\|_{\Phi}}{\|\beta_0 - \beta\|_{\Phi}} \leq 2 \left(\frac{\sqrt{\nu_{m+1}/\nu_p} - 1}{\sqrt{\nu_{m+1}/\nu_p} + 1} \right)^{m'}, \quad (\text{A.21})$$

where ν_j denotes the j -th largest eigenvalue of Φ . By Theorem 2.5, we know that

$$1 \leq \nu_p \leq \nu_{m+1} \leq 1 + \min_{k+\ell=m} \tau^2 \lambda_{(k+1)}^2 \nu_{\ell+1} ((\mathbf{X}^\top \Omega \mathbf{X})_{(-k)}) = \tilde{\kappa}_m \quad (\text{A.22})$$

and hence that $\nu_{m+1}/\nu_p \leq \tilde{\kappa}_m$. Since the function $\kappa \rightarrow (\sqrt{\kappa} - 1)/(\sqrt{\kappa} + 1)$ is increasing in κ , we can upper bound the right-hand side of (A.21) in terms of $\tilde{\kappa}_m$, yielding the desired inequality (2.15). \square

PROOF (THEOREM 2.5). We prove the more general inequality (2.14). The lower bound $1 \leq \nu_{k+\ell}(\tilde{\Phi})$ is an immediate consequence of Proposition A.1. For the upper bound, first note that $\nu_{k+\ell}(\tilde{\Phi}) \leq \nu_{\ell}(\tilde{\Phi}_{(-k)})$ by the Poincaré separation theorem (Theorem A.2). From the expression (2.11) for $\tilde{\Phi}$, we have

$$\begin{aligned} \nu_{\ell}(\tilde{\Phi}_{(-k)}) &= \nu_{\ell} \left(\mathbf{I}_k + \tau^2 \mathbf{\Lambda}_{(-k)} (\mathbf{X}^\top \Omega \mathbf{X})_{(-k)} \mathbf{\Lambda}_{(-k)} \right) \\ &= 1 + \tau^2 \nu_{\ell} \left(\mathbf{\Lambda}_{(-k)} (\mathbf{X}^\top \Omega \mathbf{X})_{(-k)} \mathbf{\Lambda}_{(-k)} \right), \end{aligned} \quad (\text{A.23})$$

where the second equality follows from Proposition A.1. Applying Lemma A.3 with $\mathbf{A} = (\mathbf{X}^\top \Omega \mathbf{X})_{(-k)}$ and $\mathbf{B} = \lambda_{(k+1)}^{-2} \mathbf{\Lambda}_{(-k)}^2$, we obtain

$$\nu_{\ell}(\tilde{\Phi}_{(-k)}) \leq 1 + \tau^2 \lambda_{(k+1)}^2 \nu_{\ell}((\mathbf{X}^\top \Omega \mathbf{X})_{(-k)}). \quad (\text{A.24})$$

Thus we have shown

$$\nu_{k+\ell}(\tilde{\Phi}) \leq 1 + \tau^2 \lambda_{(k+1)}^2 \nu_\ell((\mathbf{X}^\top \Omega \mathbf{X})_{(-k)}) \leq 1 + \tau^2 \lambda_{(k+1)}^2 \nu_\ell(\mathbf{X}^\top \Omega \mathbf{X}), \quad (\text{A.25})$$

where the inequality $\nu_\ell((\mathbf{X}^\top \Omega \mathbf{X})_{(-k)}) \leq \nu_\ell(\mathbf{X}^\top \Omega \mathbf{X})$ follows again from the Poincaré separation theorem. \square

PROPOSITION A.1. *Given a $p \times p$ symmetric matrix \mathbf{A} , the eigenvalues of the matrix $\mathbf{I}_p + \mathbf{A}$ are given by $1 + \nu_k(\mathbf{A})$ for $k = 1, \dots, p$.*

PROOF. The result follows immediately from the spectral theorem for normal matrices (Horn and Johnson, 2012). \square

THEOREM A.2 (POINCARÉ SEPARATION THEOREM). *For a given $p \times p$ symmetric matrix \mathbf{A} , let $\mathbf{A}_{(-k)}$ denote the sub-matrix with the first k rows and columns removed from \mathbf{A} . Then the eigenvalues of \mathbf{A} and $\mathbf{A}_{(-k)}$ satisfies*

$$\nu_{k+\ell}(\mathbf{A}) \leq \nu_\ell(\mathbf{A}_{(-k)}) \leq \nu_\ell(\mathbf{A}) \quad \text{for } \ell = 1, \dots, p - k. \quad (\text{A.26})$$

Since permuting the rows and columns of \mathbf{A} does not change its eigenvalues, the above inequality in fact holds for any sub-matrix of \mathbf{A} obtained by removing k rows and columns of \mathbf{A} corresponding to a common set of indices j_1, \dots, j_k .

PROOF. See Chapter 4.3 of Horn and Johnson (2012). \square

LEMMA A.3. *Let \mathbf{A} and \mathbf{B} be $p \times p$ symmetric positive definite matrices and suppose that the largest eigenvalue of \mathbf{B} satisfies $\nu_1(\mathbf{B}) \leq 1$. Then we have*

$$\nu_k(\mathbf{B}^{1/2} \mathbf{A} \mathbf{B}^{1/2}) \leq \nu_k(\mathbf{A}) \quad \text{for } k = 1, \dots, p \quad (\text{A.27})$$

where $\nu_k(\cdot)$ denotes the k -th largest eigenvalue of a given matrix.

PROOF. The result follows immediately from Ostrowski's theorem (Theorem 4.5.9 in Horn and Johnson (2012)). \square

Appendix B Theories behind convergence behavior of CG

In this section, we provide mathematical foundations behind the claims made in Rule of Thumb 2.4. In essence, Rule of Thumb 2.4 is our attempt at describing a phenomenon known as the *super-linear* convergence of CG in a quantitative yet accessible manner. While this is a well-known phenomenon among the researchers in scientific computing, it is rarely explained in canonical textbooks and reference books in numerical linear algebra.‡ Here we bring together some of the most practically useful results found in the literature and present them in a concise and self-contained manner. Our presentation in Section B.1 and B.2 is roughly based on Section 5.3 of Van der Vorst (2003) with details modified, added, and condensed

‡For example, discussions beyond Theorem 2.2 and 2.3 cannot be found in, to name a few, Trefethen and Bau (1997), Demmel (1997), Saad (2003), and Golub and Van Loan (2012).

as needed. More comprehensive treatment of the known results related to CG is found in Meurant (2006). Kuijlaars (2006) sheds additional light on CG convergence behaviors by studying them from the potential theory perspective.

Section B.1 explains the critical first step in understanding the convergence of CG applied to a positive definite system $\Phi\beta = \mathbf{b}$ — relating the CG approximation error to a polynomial interpolation error over the set $\{\nu_1, \dots, \nu_p\}$ comprising the eigenvalues of Φ . Equipped with this perspective, one can understand Theorem 2.2 as a generic and crude bound, ignoring the distributions of ν_j 's in-between the largest and smallest eigenvalues (Theorem B.3). Theorem 2.3 similarly follows from the polynomial approximation perspective.

The effects of the largest eigenvalues on CG convergence, as stated in Rule of Thumb 2.4, is made mathematically precise in Theorem B.4. Analyzing how the smallest eigenvalues delay CG convergence is more involved and requires a discussion of how the eigenvalues are approximated in the Krylov subspace. The amount of initial delay in CG convergence is closely related to how quickly these eigenvalue approximations converge. A precise statement is given in Theorem B.5.

Section B.3 provides the proofs of all the results stated in this section.

B.1 CG approximation error as polynomial approximation error

The space of polynomials \mathcal{P}_k as defined below plays a prominent role in the behavior of a worst-case CG approximation error:

$$\mathcal{P}_k = \{Q_k(\nu) : Q_k \text{ is a polynomial of degree } k \text{ with } Q_k(0) = 1\}. \quad (\text{B.28})$$

Proposition B.1 below establishes the connection between CG and the space \mathcal{P}_k .

PROPOSITION B.1. *The difference between the k -th CG iterate β_k and the exact solution β can be expressed as*

$$\beta_k - \beta = R_k(\Phi)(\beta_0 - \beta) \quad \text{for } R_k = \operatorname{argmin}_{Q_k \in \mathcal{P}_k} \|Q_k(\Phi)(\beta_0 - \beta)\|_{\Phi}. \quad (\text{B.29})$$

In particular, the following inequality holds for any $Q_k \in \mathcal{P}_k$:

$$\|\beta_k - \beta\|_{\Phi} \leq \|Q_k(\Phi)(\beta_0 - \beta)\|_{\Phi}. \quad (\text{B.30})$$

Theorem B.2 below uses Proposition B.1 to establish the relation between the CG approximation error and a polynomial interpolation error. We can interpret the result as saying the following: a worst-case CG approximation error can be quantified via how well the set of points $\{(\nu_j, 0)\}_{j=1, \dots, p}$ can be interpolated by the graph $\nu \rightarrow (\nu, Q_k(\nu))$ of a k -th degree polynomial Q_k with the constraint $Q_k(0) = 1$.

THEOREM B.2.

$$\frac{\|\beta_k - \beta\|_{\Phi}}{\|\beta_0 - \beta\|_{\Phi}} \leq \min_{Q_k \in \mathcal{P}_k} \max_{j=1, \dots, p} |Q_k(\nu_j)|, \quad (\text{B.31})$$

where ν_j denotes the j -th largest eigenvalue of Φ . The bound is sharp in a sense that, for each k , there exists an initial vector β_0 for which the equality holds.

B.2 Characterizing CG approximation error via polynomial approximation

We now derive bounds on the CG approximation error through its characterization as a polynomial interpolation error (Theorem B.2). Minimizing an interpolation error over an entire interval yields the following bound.

THEOREM B.3.

$$\min_{Q_k \in \mathcal{P}_k} \max_{\nu \in [\nu_{\min}, \nu_{\max}]} |Q_k(\nu)| \leq 2 \left(\frac{\sqrt{\nu_{\max}/\nu_{\min}} - 1}{\sqrt{\nu_{\max}/\nu_{\min}} + 1} \right)^k. \quad (\text{B.32})$$

Theorem B.2 and B.3 together yield the well-known CG approximation error bound of Theorem 2.2. As the bound of Theorem B.2 depends only on the maximum over a discrete set of the eigenvalues $\{\nu_p, \dots, \nu_1\}$, rather than the entire interval $[\nu_p, \nu_1]$, the actual CG convergence rate can be faster.

Theorem B.4 below is a basis of the following claim made in Rule of Thumb 2.4: “the r largest eigenvalues are effectively removed within r iterations.”

THEOREM B.4. *The following bound holds for all $r, k \geq 0$ with $r < p$:*

$$\frac{\|\beta_{r+k} - \beta\|_{\Phi}}{\|\beta_0 - \beta\|_{\Phi}} = \min_{Q_{r+k} \in \mathcal{P}_{r+k}} \max_{j=1, \dots, p} |Q_{r+k}(\nu_j)| \leq 2 \left(\frac{\sqrt{\nu_{r+1}/\nu_p} - 1}{\sqrt{\nu_{r+1}/\nu_p} + 1} \right)^k, \quad (\text{B.33})$$

where the first equality is given by Theorem B.2.

The smallest eigenvalues affect the CG convergence rate differently from the largest ones due to the constraint $Q_k(0) = 1$ in \mathcal{P}_k . Intuitively, this constraint makes the smallest eigenvalues more significant contributors to the polynomial interpolation error because it competes with the objective of minimizing $|Q_k(\nu)|$ for small ν . This is why we state in Rule of Thumb 2.4 that “the same number of smallest eigenvalues tends to delay the convergence longer.” Nonetheless, the effects of the smallest eigenvalues on the CG approximation error becomes attenuated as the CG iterations proceed. To quantify this phenomenon, we need to introduce the notion of *Ritz values* and describe their roles in the CG convergence behavior.

In the context of CG, the Ritz values at the k -th CG iteration refer to the roots $\{\widehat{\nu}_1^{(k)}, \dots, \widehat{\nu}_k^{(k)}\}$ of the optimal CG polynomial R_k as defined in (B.29). Unless the eigenvalues ν_p, \dots, ν_1 are distributed in a highly unusual manner, the largest and smallest ritz values have a property that they converges quickly to the largest and smallest eigenvalues of Φ (Trefethen and Bau, 1997; Driscoll et al., 1998; Kuijlaars, 2006). More precisely, we have $\widehat{\nu}_i^{(k)} \rightarrow \nu_i$ for $i = 1, \dots, r$ and $\widehat{\nu}_{k-i}^{(k)} \rightarrow \nu_{p-i}$ for $i = 0, \dots, s$ as $k \rightarrow p$. While the convergence rates of the Ritz values can be shown to be exponential, in practice quite a large number of CG iterations may be required to obtain good approximations unless $\max\{r, s\} \ll p$ (Saad, 2011).

Theorem B.5 below quantifies how the convergence of the Ritz values are related to the subsequent acceleration of the CG convergence rates.

THEOREM B.5. *The CG approximation error of the $(k + \ell)$ -th iterate relative to the k -th iterate satisfies the following bound:*

$$\frac{\|\beta_{k+\ell} - \beta\|_{\Phi}}{\|\beta_k - \beta\|_{\Phi}} \leq C_{k,r,s} 2 \left(\frac{\sqrt{\nu_{r+1}/\nu_{p-s}} - 1}{\sqrt{\nu_{r+1}/\nu_{p-s}} + 1} \right)^{\ell}, \quad (\text{B.34})$$

where $C_{k,r,s} = C_{k,r,s}(\widehat{\nu}_1^{(k)}, \dots, \widehat{\nu}_k^{(k)}) \rightarrow 1$ as $k \rightarrow p$ for any fixed $r, s \geq 0$ with $r + s < p$. More precisely, $C_{k,r,s}$ tends to 1 as the r largest and s smallest Ritz values converge to the largest and smallest eigenvalues of Φ .

B.3 Proofs for Section B

PROOF (PROPOSITION B.1). As discussed in Section 2.2, the k -th CG iterate belongs to an affine space $\beta_0 + \mathcal{K}(\Phi, \mathbf{r}_0, k)$ with $\mathbf{r}_0 = \Phi\beta_0 - \mathbf{b} = \Phi(\beta_0 - \beta)$. An element β' of the affine space can be written as

$$\beta' = \beta_0 + \sum_{\ell=1}^k c_{\ell} \Phi^{\ell-1} \mathbf{r}_0 = \beta + (\beta_0 - \beta) + \sum_{\ell=1}^k c_{\ell} \Phi^{\ell} (\beta_0 - \beta) \quad (\text{B.35})$$

for some c_1, \dots, c_k . In other words, for any β' in the affine space we can write

$$\beta' - \beta = Q_k(\Phi) (\beta_0 - \beta) \quad (\text{B.36})$$

for some $Q_k \in \mathcal{P}_k$. Together with the optimality property (2.7) of the CG iterates, the representation (B.36) implies

$$\|\beta_k - \beta\|_{\Phi} = \|R_k(\Phi)(\beta_0 - \beta)\|_{\Phi} = \min_{\beta' \in \beta_0 + \mathcal{K}(\Phi, \mathbf{r}_0, k)} \|\beta' - \beta\|_{\Phi}. \quad \square \quad (\text{B.37})$$

PROOF (THEOREM B.2). Let $\mathbf{v}_1, \dots, \mathbf{v}_p$ be the unit eigenvectors of Φ associated with the eigenvalues ν_1, \dots, ν_p . By the spectral theorem for normal matrices (Section 2.5 of Horn and Johnson (2012)), the unit eigenvectors form an orthonormal basis. In particular, we can write $\beta_0 - \beta = \sum_{j=1}^p c_j \mathbf{v}_j$ for $c_j = \langle \beta_0 - \beta, \mathbf{v}_j \rangle$. Observe that, for any $Q_k \in \mathcal{P}_k$,

$$\Phi^{1/2} Q_k(\Phi) (\beta_0 - \beta) = \sum_{j=1}^p c_j \Phi^{1/2} Q_k(\Phi) \mathbf{v}_j = \sum_{j=1}^p c_j \nu_j^{1/2} Q_k(\nu_j) \mathbf{v}_j. \quad (\text{B.38})$$

Together with (B.30), the above equality yields

$$\|\beta_k - \beta\|_{\Phi}^2 \leq \sum_{j=1}^p c_j^2 \nu_j Q_k(\nu_j)^2 \leq \max_{j=1, \dots, p} Q_k(\nu_j)^2 \left(\sum_{j=1}^p c_j^2 \nu_j \right). \quad (\text{B.39})$$

The result (B.31) follows from the above inequality since $\|\beta_0 - \beta\|_{\Phi}^2 = \sum_{j=1}^p c_j^2 \nu_j$.

The sharpness of the upper bound is proven by explicitly constructing an initial vector that achieves the bound; see Greenbaum (1979). \square

PROOF (THEOREM B.3). We can construct a shifted and scaled Chebyshev polynomial $P_k \in \mathcal{P}_k$ such that $|P_k(\nu)|$ is bounded by the right-hand side of (B.32) over the interval $[\nu_{\min}, \nu_{\max}]$. See Saad (2011) for further details. \square

PROOF (THEOREM B.4). Let Q_k^* denote the minimizer of $\max_{j=r+1, \dots, p} |Q_k(\nu_j)|$ over \mathcal{P}_k and define

$$Q'_{r+k}(\nu) = Q_k^*(\nu) \prod_{i=1}^r \left(\frac{\nu_i - \nu}{\nu_i} \right). \quad (\text{B.40})$$

Then Q'_{r+k} satisfies $Q'_{r+k}(\nu_j) = 0$ for $j = 1, \dots, r$ and $Q'_{r+k}(\nu_j) \leq Q_k^*(\nu_j)$ for $j = r+1, \dots, p$. In particular, Q'_{r+k} satisfies

$$\max_{j=1, \dots, p} |Q'_{r+k}(\nu_j)| \leq \max_{j=r+1, \dots, p} |Q_k^*(\nu_j)| = \min_{Q_k \in \mathcal{P}_k} \max_{j=r+1, \dots, p} |Q_k(\nu_j)|, \quad (\text{B.41})$$

where the equality holds as we chose Q_k^* to be the minimizer. From the above inequality, it follows that

$$\min_{Q_{r+k} \in \mathcal{P}_{r+k}} \max_{j=1, \dots, p} |Q_{r+k}(\nu_j)| \leq \max_{j=1, \dots, p} |Q'_{r+k}(\nu_j)| \leq \min_{Q_k \in \mathcal{P}_k} \max_{j=r+1, \dots, p} |Q_k(\nu_j)|. \quad (\text{B.42})$$

Since the maximum taken over an interval $[\nu_p, \nu_{r+1}]$ is larger than that over its subset, (B.42) implies

$$\min_{Q_{r+k} \in \mathcal{P}_{r+k}} \max_{j=1, \dots, p} |Q_{r+k}(\nu_j)| \leq \min_{Q_k \in \mathcal{P}_k} \max_{\nu \in [\nu_p, \nu_{r+1}]} |Q_k(\nu)|. \quad (\text{B.43})$$

The desired inequality (B.33) follows by bounding the right-hand side of (B.43) via Theorem B.3. \square

PROOF (THEOREM B.5). We first prove the bound (B.34) for $C_{k,r,s}$ as defined in (B.46) below. Let R_k be the optimal CG polynomial at the k -th iteration as defined in B.29. Since $R_k(0) = 1$, the polynomial $R_k(\nu)$ can be expressed in terms of its roots $\hat{\nu}_1^{(k)}, \dots, \hat{\nu}_k^{(k)}$ as

$$R_k(\nu) = \prod_{i=1}^k \left(\frac{\hat{\nu}_i^{(k)} - \nu}{\hat{\nu}_i^{(k)}} \right). \quad (\text{B.44})$$

Now consider $Q_k \in \mathcal{P}_k$ such that

$$Q_k(\nu) = \prod_{i=1}^r \left(\frac{\nu_i - \nu}{\nu_i} \right) \prod_{i=0}^{s-1} \left(\frac{\nu_{p-i} - \nu}{\nu_{p-i}} \right) \prod_{i=r+1}^{k-s} \left(\frac{\hat{\nu}_i^{(k)} - \nu}{\hat{\nu}_i^{(k)}} \right) \quad (\text{B.45})$$

and define

$$C_{k,r,s} = \max_{j=r+1, \dots, p-s} Q_k(\nu_j) / R_k(\nu_j). \quad (\text{B.46})$$

As in the proof of Theorem B.2, write $\beta_0 - \beta = \sum_{j=1}^p c_j \mathbf{v}_j$ so that $\beta_k - \beta = \sum_{j=1}^p c_j R_k(\nu_j) \mathbf{v}_j$. Let β'_k be a modification of β_k such that

$$\beta'_k - \beta = \sum_{j=r+1}^{p-s} c_j R_k(\nu_j) \mathbf{v}_j. \quad (\text{B.47})$$

Choose $R'_\ell \in \mathcal{P}_\ell$ to be a minimizer of $\|Q_\ell(\Phi)(\beta'_k - \beta)\|_\Phi$ over $Q_\ell \in \mathcal{P}_\ell$ or, equivalently, the optimal CG polynomial (B.29) at the ℓ -th iteration when the initial vector is taken to be β'_k . Since $\beta_{k+\ell}$ minimizes the Φ -norm over the $(k + \ell)$ -th polynomial of degree by Proposition B.1, we have

$$\|\beta_{k+\ell} - \beta\|_\Phi \leq \|R'_\ell(\Phi)Q_k(\Phi)(\beta_0 - \beta)\|_\Phi. \quad (\text{B.48})$$

We will now show that the right-hand side of (B.48) is bounded above by that of (B.34). By our definition of β'_k and $C_{k,r,s}$ in (B.47) and (B.46), we have

$$\begin{aligned} \|R'_\ell(\Phi)Q_k(\Phi)(\beta_0 - \beta)\|_\Phi^2 &= \sum_{j=r+1}^{p-s} \nu_j c_j^2 R'_\ell(\nu_j)^2 Q_k(\nu_j)^2 \\ &\leq C_{k,r,s}^2 \sum_{j=r+1}^{p-s} \nu_j c_j^2 R'_\ell(\nu_j)^2 R_k(\nu_j)^2 \\ &= C_{k,r,s}^2 \|R'_\ell(\Phi)(\beta'_k - \beta)\|_\Phi^2. \end{aligned} \quad (\text{B.49})$$

Noting that $\|\beta'_k - \beta\|_\Phi \leq \|\beta_k - \beta\|_\Phi$, we obtain

$$\|R'_\ell(\Phi)Q_k(\Phi)(\beta_0 - \beta)\|_\Phi \leq C_{k,r,s} \frac{\|R'_\ell(\Phi)(\beta'_k - \beta)\|_\Phi}{\|\beta'_k - \beta\|_\Phi} \|\beta_k - \beta\|_\Phi. \quad (\text{B.50})$$

By our choice of R'_ℓ , the vector $R'_\ell(\Phi)(\beta'_k - \beta)$ coincides with the residual of the ℓ -th CG iterate starting from the initial vector β'_k . Therefore, by Lemma B.6 combined with Theorem B.3, we have

$$\frac{\|R'_\ell(\Phi)(\beta'_k - \beta)\|_\Phi}{\|\beta'_k - \beta\|_\Phi} \leq 2 \left(\frac{\sqrt{\nu_{r+1}/\nu_{p-s}} - 1}{\sqrt{\nu_{r+1}/\nu_{p-s}} + 1} \right)^\ell. \quad (\text{B.51})$$

The claimed inequality (B.34) now follows from (B.48), (B.50), and (B.51).

Now we turn to proving the claimed property of $C_{k,r,s}$. Note that

$$\frac{Q_k(\nu)}{R_k(\nu)} = \prod_{i=1}^r \frac{\widehat{\nu}_i^{(k)}}{\nu_i} \left(\frac{\nu_i - \nu}{\widehat{\nu}_i^{(k)} - \nu} \right) \prod_{i=0}^{s-1} \frac{\widehat{\nu}_{k-i}^{(k)}}{\nu_{p-i}} \left(\frac{\nu_{p-i} - \nu}{\widehat{\nu}_{k-i}^{(k)} - \nu} \right). \quad (\text{B.52})$$

The rest of the proof focuses on the case $r = 1$ and $s = 0$ for clarity's sake; the proof remains essentially identical in the general case except for extra notational clutters. Under this case, we have

$$\max_{j=2, \dots, p} \left| \frac{Q_k(\nu_j)}{R_k(\nu_j)} \right| = \frac{\widehat{\nu}_1^{(k)}}{\nu_1} \max_{j=2, \dots, p} \left| \frac{\nu_1 - \nu_j}{\widehat{\nu}_1^{(k)} - \nu_j} \right| = \frac{\widehat{\nu}_1^{(k)}}{\nu_1} \max_{j=2, \dots, p} \left| 1 - \frac{\widehat{\nu}_1^{(k)} - \nu_1}{\nu_j - \nu_1} \right|^{-1}. \quad (\text{B.53})$$

Provided $|\widehat{\nu}_1^{(k)} - \nu_1| = \min_{j=1, \dots, p} |\widehat{\nu}_1^{(k)} - \nu_j|$, the above inequality simplifies to

$$\max_{j=2, \dots, p} \left| \frac{Q_k(\nu_j)}{R_k(\nu_j)} \right| = \frac{\widehat{\nu}_1^{(k)}}{\nu_1} \left| 1 - \frac{\widehat{\nu}_1^{(k)} - \nu_1}{\nu_2 - \nu_1} \right|^{-1}. \quad (\text{B.54})$$

So we have $C_{k,r,s} \rightarrow 1$ as $\widehat{\nu}_1^{(k)} \rightarrow \nu_1$ in the case $r = 1$ and $s = 0$. \square

LEMMA B.6. Let (ν_j, \mathbf{v}_j) for $j = 1, \dots, p$ denote the eigenvalue and eigenvector pairs of Φ . If the initial vector β_0 satisfies $\langle \beta_0 - \beta, \mathbf{v}_j \rangle = 0$ for $j \in J \subset \{1, \dots, p\}$, then the bound (B.31) holds over the set $\{1, \dots, p\} \setminus J$ i.e.

$$\frac{\|\beta_k - \beta\|_{\Phi}}{\|\beta_0 - \beta\|_{\Phi}} \leq \min_{Q_k \in \mathcal{P}_k} \max_{j \notin J} |Q_k(\nu_j)|. \quad (\text{B.55})$$

PROOF. The proof is identical to that of Theorem B.2 except that we can replace the bound (B.39) with

$$\|\beta_k - \beta\|_{\Phi}^2 \leq \sum_{j \notin J} c_j^2 \nu_j Q_k(\nu_j)^2 \leq \max_{j \notin J} Q_k(\nu_j)^2 \left(\sum_{j \notin J} c_j^2 \nu_j \right) \quad (\text{B.56})$$

since $c_j = 0$ for $j \in J$ by assumption. \square

References

- Berger, J. O., Bernardo, J. M., Sun, D. et al. (2009) The formal definition of reference priors. *The Annals of Statistics*, **37**, 905–938.
- Bhadra, A., Datta, J., Polson, N. G. and Willard, B. T. (2017) Lasso meets horseshoe. *arXiv:1706.10179*.
- Bhattacharya, A., Chakraborty, A. and Mallick, B. K. (2016) Fast sampling with Gaussian scale mixture priors in high-dimensional regression. *Biometrika*, **103**, 985–991.
- Bhattacharya, A., Pati, D., Pillai, N. S. and Dunson, D. B. (2015) Dirichlet–Laplace priors for optimal shrinkage. *Journal of the American Statistical Association*, **110**, 1479–1490.
- Carvalho, C. M., Polson, N. G. and Scott, J. G. (2010) The horseshoe estimator for sparse signals. *Biometrika*, **97**, 465–480.
- Datta, J., Ghosh, J. K. et al. (2013) Asymptotic properties of Bayes risk for the horseshoe prior. *Bayesian Analysis*, **8**, 111–132.
- Demmel, J. W. (1997) *Applied Numerical Linear Algebra*, vol. 56. Society for Industrial and Applied Mathematics.
- Dongarra, J., Heroux, M. A. and Luszczek, P. (2016) High-performance conjugate-gradient benchmark: A new metric for ranking high-performance computing systems. *The International Journal of High Performance Computing Applications*, **30**, 3–10.
- Driscoll, T. A., Toh, K.-C. and Trefethen, L. N. (1998) From potential theory to matrix iterations in six steps. *SIAM review*, **40**, 547–578.
- Duff, I. S., Erisman, A. M. and Reid, J. K. (2017) *Direct methods for sparse matrices*. Oxford University Press.

- Geyer, C. (2011) Introduction to Markov chain Monte Carlo. In *Handbook of Markov Chain Monte Carlo*, 3–48. CRC Press.
- Ghosh, J., Li, Y., Mitra, R. et al. (2018) On the use of Cauchy prior distributions for Bayesian logistic regression. *Bayesian Analysis*, **13**, 359–383.
- Gibbs, M. and MacKay, D. (1996) Efficient implementation of Gaussian processes. Unpublished manuscript.
- Golub, G. H. and Van Loan, C. F. (2012) *Matrix computations*, vol. 3. Johns Hopkins University Press.
- Graham, D. J., Reichman, M. E., Wernecke, M., Zhang, R., Southworth, M. R., Levenson, M., Sheu, T.-C., Mott, K., Goulding, M. R., Houstoun, M. et al. (2015) Cardiovascular, bleeding, and mortality risks in elderly Medicare patients treated with dabigatran or warfarin for non-valvular atrial fibrillation. *Circulation*, **131**, 157–164.
- Greenbaum, A. (1979) Comparison of splittings used with the conjugate gradient algorithm. *Numerische Mathematik*, **33**, 181–193.
- Hahn, P. R., He, J. and Lopes, H. F. (2018) Efficient sampling for Gaussian linear regression with arbitrary priors. *Journal of Computational and Graphical Statistics*.
- Hastie, T., Tibshirani, R. and Friedman, J. (2009) *The Elements of Statistical Learning*. Springer Series in Statistics. Springer.
- Hestenes, M. R. and Stiefel, E. (1952) Methods of conjugate gradients for solving linear systems. *Journal of Research of the National Bureau of Standards*, **49**.
- Horn, R. A. and Johnson, C. R. (2012) *Matrix Analysis*. Cambridge University Press.
- Hripcsak, G., Duke, J. D., Shah, N. H., Reich, C. G., Huser, V., Schuemie, M. J., Suchard, M. A., Park, R. W., Wong, I. C. K., Rijnbeek, P. R. et al. (2015) Observational Health Data Sciences and Informatics (OHDSI): Opportunities for observational researchers. *Studies in health technology and informatics*, **216**, 574.
- Johndrow, J. E., Orenstein, P. and Bhattacharya, A. (2018) Bayes shrinkage at GWAS scale: Convergence and approximation theory of a scalable MCMC algorithm for the horseshoe prior. *arXiv:1705.00841*.
- Jolliffe, I. T. (2002) *Principal Component Analysis*. Springer Series in Statistics. Springer.
- Kuijlaars, A. B. J. (2006) Convergence analysis of Krylov subspace iterations with methods from potential theory. *SIAM review*, **48**, 3–40.
- Kyung, M., Gill, J., Ghosh, M., Casella, G. et al. (2010) Penalized regression, standard errors, and Bayesian lassos. *Bayesian Analysis*, **5**, 369–411.

- Lanczos, C. (1952) Solution of systems of linear equations by minimized iterations. *Journal of Research of the National Bureau of Standards*, **49**, 33–53.
- Meurant, G. A. (2006) *The Lanczos and Conjugate Gradient Algorithms: from Theory to Finite Precision Computations*. Society for Industrial and Applied Mathematics.
- Pal, S., Khare, K. et al. (2014) Geometric ergodicity for Bayesian shrinkage models. *Electronic Journal of Statistics*, **8**, 604–645.
- Park, T. and Casella, G. (2008) The Bayesian Lasso. *Journal of the American Statistical Association*, **103**, 681–686.
- Piironen, J. and Vehtari, A. (2017) Sparsity information and regularization in the horseshoe and other shrinkage priors. *arXiv:1707.01694*.
- Plummer, M., Best, N., Cowles, K. and Vines, K. (2006) Coda: convergence diagnosis and output analysis for MCMC. *R news*, **6**, 7–11.
- Polson, N. G., Scott, J. G. and Windle, J. (2013) Bayesian inference for logistic models using Pólya–Gamma latent variables. *Journal of the American Statistical Association*, **108**, 1339–1349.
- (2014) The Bayesian bridge. *Journal of the Royal Statistical Society: Series B (Statistical Methodology)*, **76**, 713–733.
- Rue, H. and Held, L. (2005) *Gaussian Markov random fields: theory and applications*. CRC press.
- Saad, Y. (2003) *Iterative Methods for Sparse Linear Systems*, vol. 82. Society for Industrial and Applied Mathematics.
- (2011) *Numerical Methods for Large Eigenvalue Problems: Revised Edition*. Classics in Applied Mathematics. Society for Industrial and Applied Mathematics.
- Schuemie, M. J., Ryan, P. B., Hripcsak, G., Madigan, D. and Suchard, M. A. (2018a) Improving reproducibility by using high-throughput observational studies with empirical calibration. *Philosophical Transactions of the Royal Society of London A: Mathematical, Physical and Engineering Sciences*, **376**, 20170356.
- (2018b) A systematic approach to improving the reliability and scale of evidence from health care data. *arXiv:1803.10791*.
- Stein, M. L., Chen, J. and Anitescu, M. (2012) Difference filter preconditioning for large covariance matrices. *SIAM Journal on Matrix Analysis and Applications*, **33**, 52–72.
- Stroud, J. R., Stein, M. L. and Lysen, S. (2017) Bayesian and maximum likelihood estimation for Gaussian processes on an incomplete lattice. *Journal of Computational and Graphical Statistics*, **26**, 108–120.
- Stuart, E. A. (2010) Matching methods for causal inference: A review and a look forward. *Statistical Science*, **25**, 1.

- Sun, Y. and Stein, M. L. (2016) Statistically and computationally efficient estimating equations for large spatial datasets. *Journal of Computational and Graphical Statistics*, **25**, 187–208.
- Tian, Y., Schuemie, M. J. and Suchard, M. A. (2018) Evaluating large-scale propensity score performance through real-world and synthetic data experiments. *International Journal of Epidemiology*.
- Trefethen, L. N. and Bau, D. (1997) *Numerical Linear Algebra*. Society for Industrial and Applied Mathematics.
- Van der Vorst, H. A. (2003) *Iterative Krylov Methods for Large Linear Systems*, vol. 13. Cambridge University Press.
- Walker, A. M., Patrick, A. R., Lauer, M. S., Hornbrook, M. C., Marin, M. G., Platt, R., Roger, V. L., Stang, P. and Schneeweiss, S. (2013) A tool for assessing the feasibility of comparative effectiveness research. *Comparative Effectiveness Research*, **3**, 11–20.
- Xu, X., Ghosh, M. et al. (2015) Bayesian variable selection and estimation for group lasso. *Bayesian Analysis*, **10**, 909–936.
- Zhang, L., Datta, A. and Banerjee, S. (2018) Practical Bayesian modeling and inference for massive spatial datasets on modest computing environments. *arXiv:1802.00495*.
- Zhou, Q. and Guan, Y. (2017) Fast model-fitting of Bayesian variable selection regression using the iterative complex factorization algorithm. *arXiv preprint arXiv:1706.09888*.

Supplement to “Prior-preconditioned conjugate gradient for accelerated Gibbs sampling in “large n & large p ” sparse Bayesian regression models”

S1. General principle behind the prior-preconditioning approach

In the context of the CG sampler, the preconditioned matrix $\mathbf{M}^{-1/2}\tilde{\Phi}\mathbf{M}^{-1/2}$ represents the precision matrix of the transformed parameter $\tilde{\beta} = \mathbf{M}^{1/2}\beta$. In fact, preconditioning the linear system (2.5) with a preconditioner \mathbf{M} is equivalent to applying a parameter transformation $\beta \rightarrow \mathbf{M}^{1/2}\beta$ before employing the CG sampler. That is, we can apply one of the two strategies — precondition the linear system or apply the parameter transformation — to achieve exactly the same effect on the speed of the CG sampler.

When we choose the prior precision as the preconditioner, the transformed parameter $\mathbf{M}^{1/2}\beta$ a priori has the identity precision matrix, before its distribution is modified via the likelihood. This perspective, combined with the fact that the eigenvalues of $\tilde{\Phi}$ represents the posterior precisions of $\mathbf{M}^{1/2}\beta$ along its principal components, suggests the following principle:

PRINCIPLE BEHIND PRIOR-PRECONDITIONING S1.1. Under a strongly informative prior, the posterior looks like the prior except in a small number of directions along which the data provide significant information. This translates into the eigenvalues of the prior-preconditioned matrix $\tilde{\Phi}$ clustering around 1 except for a relatively small number of large eigenvalues.

The eigenvalue structure of the prior-preconditioned matrix as predicted above is indeed observed across all of our numerical examples — see Figure 3.2, S4, and S7.

S2. Practical details on deploying the CG sampler for sparse regression

Throughout this section, we write \mathbf{vw} and \mathbf{v}/\mathbf{w} to denote an element-wise multiplication and division of two vectors \mathbf{v} and \mathbf{w} .

S2.1. Choice of the initial vector for CG iterations

Generally speaking, the CG iterations decrease the distance between the iterates β_k 's and the exact solution β relative to the initial error $\|\beta_0 - \beta\|_{\Phi}$. However, a choice of the initial vector is not as significant as that of the preconditioner which determines the eventual exponential convergence rate of CG. In other words, once the initial vector is chosen within a reasonable range, we should not expect a dramatic gain from further fine-tuning. When sampling β from a sparse regression posterior, we indeed find it difficult to improve much over a simple initialization $\beta_0 = \mathbf{0}$, which is a reasonable choice as most coefficients are shrunk to zero. We achieve only small ($\lesssim 10\%$), though consistent, improvements by one of the alternative approaches we experimented with. We describe these approaches below.

As an alternative to $\beta_0 = \mathbf{0}$, we consider three approaches for constructing the initial vector. At the m -th Gibbs update, the CG sampler needs to draw $\beta^{(m)}$ from the distribution $\beta \mid \omega^{(m-1)}, \lambda^{(m-1)}, \tau^{(m-1)}, \mathbf{y}, \mathbf{X}$. We have no control over the variability in $\beta^{(m)}$, so we focus on getting β_0 as close as possible to the mean of $\beta^{(m)}$. The two seemingly obvious choices of β_0 are 1) the previous MCMC sample $\beta^{(m-1)}$ and 2) the MCMC estimate $m^{-1} \sum_{i=0}^{m-1} \beta^{(i)}$ of the expectation $\mathbb{E}[\beta \mid \mathbf{y}, \mathbf{X}]$. These options, however, ignores the fact that the distribution of $\beta^{(m)}$ depends strongly on $\tau^{(m-1)} \lambda^{(m-1)}$, which generally is very different from $\tau^{(m-i)} \lambda^{(m-i)}$ for $i \geq 2$.

We found the following approach, used in our CG-accelerated Gibbs sampler implementation of Section 4, to yield a better estimate of the mean and hence a better initialization for $\beta^{(m)}$. We first estimate $\mathbb{E}[\tau^{-1} \lambda^{-1} \beta \mid \mathbf{y}, \mathbf{X}]$ by the estimator $\tilde{\beta}_0 = m^{-1} \sum_{i=0}^{m-1} \beta^{(i)} / \tau^{(i-1)} \lambda^{(i-1)}$, where we define $\tau^{(-1)} \lambda_j^{(-1)} = 1$. (We sample $\beta^{(i)}$ conditional on $\tau^{(i-1)}$ and $\lambda^{(i-1)}$; see Section S5.2 for further details on our Gibbs update orders.) Then we rescale it with the current conditioned values of τ and λ , setting $\beta_0 = \tau^{(m-1)} \lambda^{(m-1)} \tilde{\beta}_0$ to obtain the initial vector. We compared this approach to the other two through a simulation study and found our choice to consistently yield smaller Φ -norm errors and faster convergence.

S2.2. Termination criteria for CG iterations

An iterative method must be supplied with a termination criteria to decide when the current iterate β_k is close enough to the exact solution. While different convergence metrics can be computed as bi-products of the CG iterations (Meurant, 2006), most existing linear algebra libraries uses the ℓ^2 norm of the residual $\mathbf{r}_k = \Phi \beta_k - \mathbf{b}$. It is possible to relate the residual norm to $\|\beta_k - \beta\|_2$ as

$$\|\beta_k - \beta\|_2 = \|\Phi^{-1} \mathbf{r}_k\|_2 \leq \|\Phi^{-1}\|_2 \|\mathbf{r}_k\|_2. \quad (\text{S1})$$

For the purpose of sampling a Gaussian vector β , however, it is not at all clear when $\|\mathbf{r}_k\|_2$ or $\|\beta_k - \beta\|_2$ can be considered small enough. To address this problem, we develop an alternative metric tailored toward the CG sampler for sparse regression.

We propose to assess the CG convergence in terms of the ℓ^2 norm of the prior-preconditioned residual $\tilde{\mathbf{r}}_k = \tilde{\Phi} \tilde{\beta}_k - \tilde{\mathbf{b}} = \tau \lambda \mathbf{r}_k$. More specifically, we use the termination criteria

$$p^{-1/2} \|\tilde{\mathbf{r}}_k\|_2 = \left\{ p^{-1} \sum_{j=1}^p (\tilde{\mathbf{r}}_k)_j^2 \right\}^{1/2} \leq 10^{-6}, \quad (\text{S2})$$

in terms of the root-mean-squared residual $p^{-1/2} \|\tilde{\mathbf{r}}_k\|_2$. The criteria is justified by the norm $\|\tilde{\mathbf{r}}_k\|_2$ being an approximate upper bound to the following quantity:

$$\|\xi^{-1} (\beta_k - \beta)\|_2 \quad \text{with} \quad \xi_j^2 = \mathbb{E}[\beta_j^2 \mid \omega, \lambda, \tau, \mathbf{y}, \mathbf{X}]. \quad (\text{S3})$$

The standardization by second moment ensures that, when the computed error is small, all the coordinates of β_k are close to those of β either in terms of their means or variances of the target Gaussian distribution.

To relate the norm of the prior-preconditioned residual $\tilde{\mathbf{r}}_k = \tilde{\Phi}\tilde{\beta}_k - \tilde{\mathbf{b}}$ to the error metric (S3), observe that $\beta_k - \beta = \mathbf{M}^{-1/2}\tilde{\Phi}^{-1}\tilde{\mathbf{r}}_k$ with $\mathbf{M} = \tau^{-2}\mathbf{\Lambda}^{-2}$ and hence

$$\|\xi^{-1}(\beta_k - \beta)\|_2 = \|\xi^{-1}(\tau\lambda)(\tilde{\Phi}^{-1}\tilde{\mathbf{r}}_k)\|_2 \leq \left(\max_j \xi_j^{-1}\tau\lambda_j\right) \|\tilde{\Phi}^{-1}\tilde{\mathbf{r}}_k\|_2. \quad (\text{S4})$$

The inequality in the above equation only represents the worst-case scenario; in more typical settings, one expects the norm of $\xi^{-1}(\tau\lambda)\mathbf{v}$ to be related to that of \mathbf{v} through some average of $\xi_j^{-1}\tau\lambda_j$'s. In any case, we proceed to analyze a typical behavior of $\xi_j^{-1}\tau\lambda_j$ as the parameters ω, λ, τ are drawn from a sparse regression posterior. As before, we interpret $\tau^2\lambda_j^2$ as the prior variance of β_j (conditional on ω, λ, τ) before observing \mathbf{y}, \mathbf{X} . Note that

$$(\xi_j^{-1}\tau\lambda_j)^2 = \frac{\tau^2\lambda_j^2}{\mu_j^2 + \sigma_j^2}, \quad (\text{S5})$$

where μ_j and σ_j are the conditional mean and variance of $\beta_j | \omega, \lambda, \tau, \mathbf{y}, \mathbf{X}$. So the quantity $\xi_j^{-1}\tau\lambda_j$ is not too far from 1 if either $|\mu_j|$ or σ_j is in the same order of magnitude as $\tau\lambda_j$. If β_j 's posterior is dominated by the prior shrinkage, we expect the posterior (conditional) variance to be not much smaller than the prior one and hence $\sigma_j \approx \tau\lambda_j$. Otherwise, if $\sigma_j \ll \tau\lambda_j$ and the likelihood is a dominant contributor to the posterior, then the posterior of $\tau\lambda_j$ should concentrate around $|\mu_j|$ to maximize the marginal likelihood of $\beta_j \approx \mu_j$. Either way, we can expect $\xi_j^{-1}\tau\lambda_j$ to be in the same order of magnitude as 1.

From the relation (S4) and our analysis above, we deduce that

$$\|\xi^{-1}(\beta_k - \beta)\|_2 \lesssim \|\tilde{\Phi}^{-1}\tilde{\mathbf{r}}_k\|_2 \leq \|\tilde{\mathbf{r}}_k\|_2, \quad (\text{S6})$$

where the latter inequality follows from the fact that the largest eigenvalue of the prior-preconditioned matrix $\tilde{\Phi}^{-1}$ is bounded above by 1 by Theorem 2.5.

S2.3. Modified preconditioner to handle coefficients with uninformative priors

When fitting a sparse regression model, standard practice is to include an intercept β_0 without any shrinkage, often with the improper flat prior $\pi(\beta_0) \propto 1$ (Park and Casella, 2008). Additionally, there may be predictors of particular interests, inference for whose regression coefficients is more appropriately carried out with uninformative or weakly-informative priors without shrinkage; see Zucknick et al. (2015) as well as the application in Section 4 for examples of such predictors. The CG sampler can accommodate such predictors with an appropriate modification.

For notational convenience, suppose that the regression coefficients are indexed so that the first $(q + 1)$ -th coefficients $\beta_0, \beta_1, \dots, \beta_q$ are to be estimated without shrinkage. We further assume that the unshrunk coefficients are given independent Gaussian priors $\beta_j \sim \mathcal{N}(0, \sigma_j^2)$ for $0 < \sigma_j \leq \infty$ where $\sigma_j = \infty$ denotes an improper prior $\pi(\beta_j) \propto 1$. The precision matrix of $\beta | \omega, \lambda, \tau, \mathbf{y}, \mathbf{X}$ then is given by

$$\Phi = \mathbf{X}^\top \Omega \mathbf{X} + \begin{bmatrix} \text{diag}(\sigma)^{-2} & \mathbf{0} \\ \mathbf{0} & \tau^{-2}\mathbf{\Lambda}^{-2} \end{bmatrix} \quad (\text{S7})$$

for $\boldsymbol{\sigma} = (\sigma_0, \dots, \sigma_q)$ where we employ the convention $1/\sigma_j = 0$ if $\sigma_j = \infty$. The unshrunk coefficients β_0, \dots, β_q are distinguished from the shrunk ones by the fact that their prior scales σ_j (before conditioning on \mathbf{y} and \mathbf{X}) typically have little to do with their posterior scales (after conditioning on \mathbf{y} and \mathbf{X}). For this reason, a naively modified preconditioner $\mathbf{M} = \text{diag}(\boldsymbol{\sigma}^{-2}, \tau^{-2}\boldsymbol{\lambda}^{-2})$ may not be appropriate, especially for coefficients with $\sigma_j \gg 1$ corresponding to uninformative priors.

We propose a modified preconditioner of the form $\mathbf{M} = \text{diag}(\boldsymbol{\gamma}^{-2}, \tau^{-2}\boldsymbol{\lambda}^{-2})$ for appropriately chosen $\boldsymbol{\gamma} = (\gamma_0, \gamma_1, \dots, \gamma_q)$. For the corresponding preconditioned matrix $\tilde{\boldsymbol{\Phi}} = \mathbf{M}^{-1/2}\boldsymbol{\Phi}\mathbf{M}^{-1/2}$, let $\tilde{\boldsymbol{\Phi}}_{(-q-1)}$ denote the sub-matrix with the first $q+1$ rows and columns removed. As shown in Section 2.5, the sub-matrix $\tilde{\boldsymbol{\Phi}}_{(-q-1)}$ has an eigenvalue distribution particularly well-suited to induce rapid CG convergence. By the Poincaré separation theorem (Theorem A.2), all but $q+1$ eigenvalues of the original matrix $\tilde{\boldsymbol{\Phi}}$ lie within the largest and smallest eigenvalues of the sub-matrix $\tilde{\boldsymbol{\Phi}}_{(-q-1)}$. In choosing γ_j 's, therefore, we are concerned with the behavior of the $q+1$ additional eigenvalues introduced by the unshrunk coefficients. Additionally, we should err on the side of introducing larger eigenvalues than smaller ones as small eigenvalues impact CG convergence rates more significantly (Rule of Thumb 2.4).

With the above objectives in mind, we propose a choice

$$\gamma_j = c\hat{\psi}_j \quad \text{for} \quad \hat{\psi}_j^2 \approx \text{var}(\beta_j | \boldsymbol{\omega}, \boldsymbol{\lambda}, \tau, \mathbf{y}, \mathbf{X}) \quad \text{and} \quad c \geq 1. \quad (\text{S8})$$

To explain the reasoning behind the above choice, let $\boldsymbol{\beta}_q = (\beta_0, \dots, \beta_q)$ and $\boldsymbol{\beta}_{(-q)} = (\beta_{q+1}, \dots, \beta_p)$. The smallest eigenvalues of $\tilde{\boldsymbol{\Phi}}$ correspond to the largest variances (conditional on $\boldsymbol{\omega}, \boldsymbol{\lambda}, \tau, \mathbf{y}, \mathbf{X}$) of the Gaussian vector $\mathbf{M}^{1/2}\boldsymbol{\beta} = (\boldsymbol{\gamma}^{-1}\boldsymbol{\beta}_q, \tau^{-1}\boldsymbol{\lambda}^{-1}\boldsymbol{\beta}_{(-q)})$ along its principal components. The variances of $\tau^{-1}\boldsymbol{\lambda}^{-1}\boldsymbol{\beta}_{(-q)}$ conditional on $\boldsymbol{\gamma}^{-1}\boldsymbol{\beta}_q$ are bounded above by 1 along any directions because the eigenvalues of the conditional precision matrix $\tilde{\boldsymbol{\Phi}}_{(-q)}$ are bounded below by 1. Therefore, we do not expect $(\boldsymbol{\gamma}^{-1}\boldsymbol{\beta}_q, \tau^{-1}\boldsymbol{\lambda}^{-1}\boldsymbol{\beta}_{(-q)})$ to have variances much larger than 1 unless the marginal variances of $\boldsymbol{\gamma}^{-1}\boldsymbol{\beta}_q$ are large. The proposed choice of γ_j 's ensure that the marginal variances of $\gamma_j^{-1}\beta_j$'s are less than c^{-1} and thus prevent an introduction of small eigenvalues to $\tilde{\boldsymbol{\Phi}}$. The multiplicative factor $c \geq 1$ provides a further safeguard as we are more concerned about small eigenvalues than large ones.

As the parameters $\boldsymbol{\omega}, \tau, \boldsymbol{\lambda}$ are constantly updated during Gibbs sampling, technically we cannot estimate $\text{var}(\beta_j | \boldsymbol{\omega}, \boldsymbol{\lambda}, \tau, \mathbf{y}, \mathbf{X})$ from earlier MCMC samples. In practice, we instead use

$$\gamma_j = c\hat{\eta}_j \quad \text{for} \quad \hat{\eta}_j^2 \approx \text{var}(\beta_j | \mathbf{y}, \mathbf{X}). \quad (\text{S9})$$

Using (S9) in place of (S8) is justified in two ways. First, by the variance decomposition formula we have

$$\mathbb{E}_{\boldsymbol{\omega}, \tau, \boldsymbol{\lambda} | \mathbf{y}, \mathbf{X}} [\text{var}(\beta_j | \boldsymbol{\omega}, \boldsymbol{\lambda}, \tau, \mathbf{y}, \mathbf{X})] \leq \text{var}(\beta_j | \mathbf{y}, \mathbf{X}). \quad (\text{S10})$$

In other words, on average $\hat{\eta}_j$ is an overestimate of $\hat{\psi}_j$ which, as we have discussed, is more preferable to an underestimate. Secondly, the unshrunk coefficients β_0, \dots, β_q have only limited dependency on the shrinkage parameters τ and

λ through $\beta_{q+1}, \dots, \beta_p$. Also, in our experience we have never noticed any obvious correlations between the posterior samples of ω and β . For these reasons, we suspect that $\text{var}(\beta_j | \mathbf{y}, \mathbf{X})$ is generally not too far from $\text{var}(\beta_j | \omega, \lambda, \tau, \mathbf{y}, \mathbf{X})$.

Once chosen within reasonable ranges, the precise values of γ_j 's have limited effect on the CG convergence rate. This is because all but $(q+1)$ eigenvalues are well-behaved regardless of the choice of $\gamma_0, \dots, \gamma_q$ and CG has an ability to eventually "remove" the extreme eigenvalues (Rule of Thumb 2.4). In our simulations (not presented in the manuscript), we found the delay in the CG convergence to be no more than 20 ~ 30% even when the values of γ_j 's were off by two orders of magnitude from empirically-determined optimal values. The convergence rate achieved by the proposed choice of γ was essentially indistinguishable from that achieved by an optimal choice.

S3. Effects of error metrics and right-hand vectors on the CG sampler convergence behaviors of Section 3.3

The CG convergence behavior as illustrated in Figure 3.1 remains qualitatively consistent across different random draws of the right-hand vector \mathbf{b} and across various metrics of the approximation error. Figure S1 shows the average of the coordinate-wise relative error as a function of the CG iterations as in Figure 3.1, but with an individual line for each of the random draws of \mathbf{b} . The convergence behaviors under the prior and Jacobi preconditioners are plotted in the two separate sub-figures to avoid cluttering the plot with too many lines. Figure S2 shows the CG convergence behaviors under the two additional error metrics: the ℓ^2 -norm and Φ -norm distance between β_k and β_{direct} .

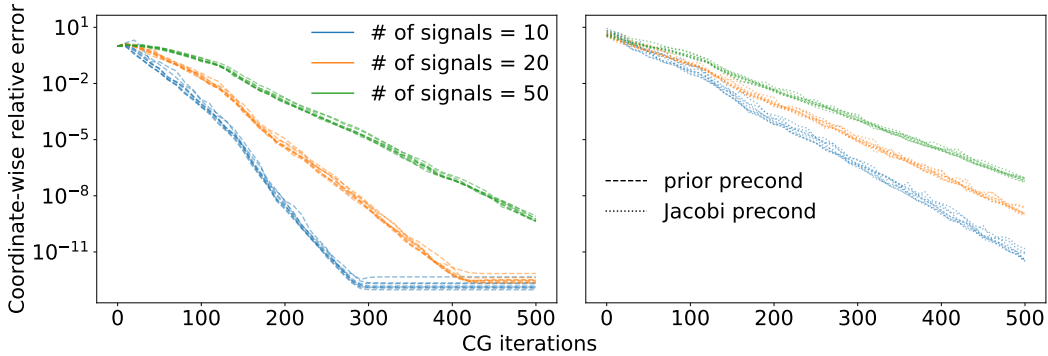


Fig. S1. Plots of the CG approximation errors (with the same error metric as used in Figure 3.1) as a function of the number of CG iterations. Shown on the left is under the prior preconditioner and on the right is under the Jacobi preconditioner. The three different colors corresponds to the three different posterior conditional distributions of β with the varying numbers of true signals. Within the same color, the different lines correspond to the different random draws of the right-hand vector \mathbf{b} generated as in (2.4).

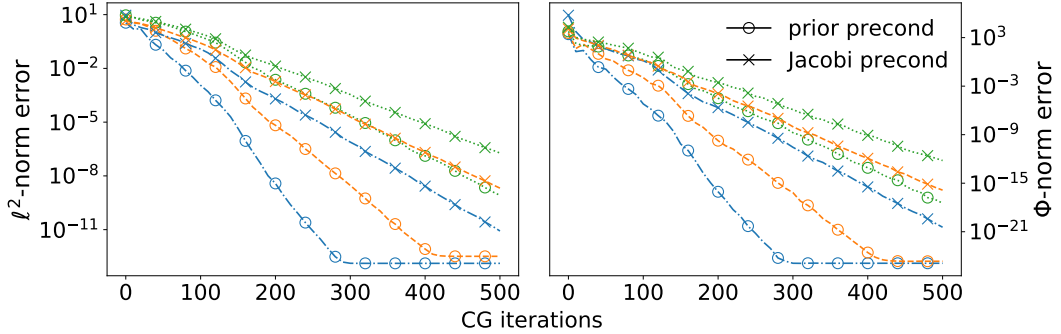


Fig. S2. Plots of the ℓ^2 -norm (on the left) and the Φ -norm (on the right) between β_k and β_{direct} as a function of the number of CG iterations. Other than the use of the two alternative error metrics for the y -axes, each of the plotted lines directly corresponds to the one with the same color and marker in Figure 3.1.

S4. Optimizing linear algebra computations for the Gibbs samplers

S4.1. Dense v.s. sparse numerical linear algebra

When a design matrix \mathbf{X} is sparse as in the application of Section 4, one may wonder if the precision matrix Φ can be factorized efficiently using sparse numerical linear algebra techniques. This is not the case in typical sparse regression applications, however, for the following reasons. First, the matrix $\mathbf{X}^\top \Omega \mathbf{X}$ and hence Φ is typically much denser than \mathbf{X} itself, especially when $n > p$. In particular, the (j, j') -th element of $\mathbf{X}^\top \Omega \mathbf{X}$ is non-zero if the j -th and j' -th predictors co-occur in any of the n samples. Secondly, when employing sparse methods, time spent on irregular data access completely dominate over that on arithmetic operations (Duff et al., 2017). In the absence of sufficient sparsity, therefore, it can be more computationally efficient to ignore the sparse structure and employ dense methods.

In the application of Section 4, we find the precision matrix Φ to be 85.4% dense. The Cholesky factor of a sparse matrix is typically denser than the matrix itself (see Theorem 2.8 in Rue and Held, 2005); indeed, we find the Cholesky factor \mathbf{L} to be over 99% dense. Sparse methods have no advantage whatsoever for such a dense matrix.

Conceivably, we can avoid dealing with the near-dense Φ matrix in (2.5) as follows. Noting that $\Phi = \tilde{\mathbf{X}}^\top \tilde{\mathbf{X}}$ for $\tilde{\mathbf{X}}^\top = [\mathbf{X}^\top, \tau^{-1} \mathbf{\Lambda}^{-1}]$, we see that a (Q -less) QR decomposition of the sparse matrix $\tilde{\mathbf{X}}$ would provide the Cholesky factor of Φ . For the application of Section 4, we experimented with this idea using the popular SparseSuites package (Davis, 2011). Sparse QR decomposition first attempts to find a permutation of the matrix columns to reduce the subsequent computation as much as possible. The package implements approximate minimum degree (AMD), column AMD (COLAMD), as well as graph-partitioning-based nested dissection (METIS) algorithm. None of these algorithms find column orderings that differ significantly from the original arbitrary ordering with only handful of columns permuted. The subsequent factorization of the matrix requires about 25 minutes regardless of the

column permutation algorithm chosen. On the other hand, explicitly computing Φ and finding its Cholesky factor via dense linear algebra requires about 3 minutes only (Section S4.2).

S4.2. Choice of a linear algebra library

For linear algebra operations involving large matrices, hardware-specific compilation and optimization are essential for achieving good computational efficiency. Major linear algebra libraries all achieve reasonable computational efficiency, but some variation in performance may occur depending on types of operations and computing environments. We therefore compare a few options for implementing the direct and CG-accelerated Gibbs sampler in Section 4. Efficiency of sparse matrix operations also depends critically on the underlying representations of sparse matrices (Saad, 2011). For each linear algebra library, we try all the major sparse matrix formats and report only the result with best performance. All the benchmarks here are run using the design matrix of Section 4.

The computational bottleneck of the direct Gibbs sampler is computing $\mathbf{X}^\top \Omega \mathbf{X}$ and the subsequent Cholesky factorization of Φ . Since Ω is a diagonal matrix, computing $\mathbf{X}^\top \Omega \mathbf{X}$ can be carried out as multiplying a sparse matrix $\mathbf{X}^\top \Omega^{1/2}$ with its transpose. The high-performance computing community refers to the operation of multiplying two sparse matrices by the acronym SpGEMM (generalized sparse matrix-matrix multiplication). SpGEMM is a surprisingly complicated operation to optimize in modern computing architectures. No specification is provided for such an operation by sparse BLAS (Duff et al., 2002), and its hardware-specific implementation is an active area of research (Matam et al., 2012; Azad et al., 2016).

The Scipy library provides an SpGEMM implementation via the algorithm of Bank and Douglas (1993). The Scipy SpGEMM operation requires 144 seconds. We find an alternative implementation in the Intel MKL library with the option of returning a dense (instead of sparse) matrix, which is faster here as the multiplied matrix is almost completely dense. The MKL SpGEMM requires 64.6 seconds, being a clear winner and our choice for the simulation results of Section 4.

For the (dense linear algebra) Cholesky factorization of Φ , the Scipy library by default calls the MKL library. The computation requires 78.0 seconds. The OpenBLAS implementation performs comparably, requiring 79.0 seconds.

The computation time of the CG-accelerated Gibbs is dominated by the (sparse) matrix-vector multiplications $\mathbf{v} \rightarrow \mathbf{X}\mathbf{v}$ and $\mathbf{w} \rightarrow \mathbf{X}^\top \mathbf{w}$ required for CG iterations. For these operations, the Scipy library uses its own C-extension code. On average, the operation $\mathbf{v} \rightarrow \mathbf{X}\mathbf{v}$ requires 6.70×10^{-2} seconds and the operation $\mathbf{w} \rightarrow \mathbf{X}^\top \mathbf{w}$ 6.07×10^{-2} seconds. With the MKL library implementations, these matrix-vector multiplications on average require 4.69×10^{-2} and 5.49×10^{-2} seconds respectively.

S4.3. Opportunities for parallelization within memory constraints

The above comparisons of computational efficiency are based on a single-threaded CPU computing environment. Computational gain from parallelization is highly architecture dependent for large-scale problems and is difficult to draw any general

conclusions (Dongarra et al., 2016; Duff et al., 2017). Nonetheless, here we provide a qualitative discussion of to what extent each algorithm can benefit from parallelization. We complement the discussion with illustrative quantitative results, obtained by using all the four Intel CPU’s of the 2015 iMac.

Before any discussion of computational gains from parallelization, we emphasize the following point regarding the two alternative Gibbs samplers for sparse Bayesian regression: as the problem size grows, memory constraints make the CG-accelerated sampler *the only option* in a typical computing environment. We can run the CG-accelerated sampler as long as we have enough memory to store the (sparse) design matrix \mathbf{X} . On the other hand, as we have discussed, the direct Gibbs sampler generally cannot avoid having to store the near-dense precision matrix Φ . In case of the sparse design matrix \mathbf{X} of size $72,489 \times 22,175$ in Section 4, for example, storing \mathbf{X} in the compressed sparse row format only requires 0.719GB of memory while storing the dense Φ requires 3.67GB of memory. In fact, further memory burden is incurred by temporary allocation of extra memory necessary for the Cholesky factorization of Φ . Profiling the memory usage by the MKL library reveal that temporary memory allocation of 3.75GB, requiring at least 8.14 ($= 0.719 + 3.67 + 3.75$) GB of memory for running the direct Gibbs sampler.

Dense linear algebra operations benefit most from parallelization when using a typical modern hardware, which performs best at accessing data stored contiguously in memory (Dongarra et al., 2016). In fact, computation time for the Cholesky factorization goes down from 78.0 to 22.7 seconds when using the four CPU’s with the MKL library. It is also worth noting that the speed-up is significantly smaller when using the OpenBLAS library; the time goes down from 79.0 only to 33.1 seconds, illustrating the importance of hardware-specific optimizations in parallel computing.

Parallelizing sparse linear algebra operations are more complex due to their bottleneck being irregular data access (Duff et al., 2017). Speed-ups thus tend to be smaller, though there are growing efforts in building hardwares optimized for sparse operations (Dongarra et al., 2016). The MKL spGEMM delivers a modest speed-up when using the four CPU’s, cutting the time from 64.6 to 46.8 seconds. The sparse matrix-vector multiplications $\mathbf{v} \rightarrow \mathbf{X}\mathbf{v}$ and $\mathbf{w} \rightarrow \mathbf{X}^T\mathbf{w}$ benefit slightly more from parallelization. The MKL library implementations reduces the time from 4.69×10^{-2} to 3.13×10^{-2} seconds and from 5.49×10^{-2} to 3.14×10^{-2} seconds respectively.

S5. In-depth look at the mechanism of CG-acceleration in Section 4

S5.1. Number of CG iterations at each Gibbs step

To study computational cost of the CG sampler at each Gibbs iteration, we first focus on a post-burn-in update of β for the propensity score model. As in Section 3, we compare the CG iterates β_k against the exact solution β_{direct} of the linear system (2.5) found via the Cholesky-based direct method. Figure S3 plots the distances between β_k and β_{direct} as a function of k , the number of CG iterations or equivalently of matrix vector multiplications $\mathbf{v} \rightarrow \Phi\mathbf{v}$.

The solid blue line tracks the root mean squared residual $p^{-1/2}\|\tilde{\mathbf{r}}_k\|_2$ as introduced in Section S2.2. The dotted vertical line indicates when the magnitude of the prior-preconditioned residual $\tilde{\mathbf{r}}_k$ falls below the termination criteria of (S2). The termination occurs at $k = 133$ and the CG sampler consequently spends less than 10% of the computational time relative to the direct sampler. Note also how the solid blue line upper-bounds the dashed one which tracks the following error metric computed as a proxy for (S3):

$$\left\{p^{-1}\sum_j \hat{\xi}_j^{-2}(\boldsymbol{\beta}_k - \boldsymbol{\beta}_{\text{direct}})_j^2\right\}^{1/2} \quad \text{with} \quad \hat{\xi}_j^2 \approx \mathbb{E}[\beta_j^2 | \mathbf{y}, \mathbf{X}]. \quad (\text{S11})$$

This empirical result provides a further support to our theoretical analysis in Section S2.2 and hence to the use of $p^{-1/2}\|\tilde{\mathbf{r}}_k\|_2$ in the termination criteria. As confirmed in Section 4.5, the CG error at termination is so small that it does not affect the stationary distribution of the Gibbs sampler in any statistically significant way.

Figure S3 also makes it clear that the advantage of the prior preconditioner, as demonstrated in the simulated data examples of Section 3, continues to hold in this real data example. The observed convergence behaviors under the two preconditioners are again well explained by the eigenvalue distributions of the respective preconditioned matrices (Figure S4); prior preconditioning leads to a tighter cluster of the eigenvalues and avoids introducing small eigenvalues.

The number of required CG iterations depends on the random quantities $\boldsymbol{\omega}$, τ , $\boldsymbol{\lambda}$, and \mathbf{b} and hence fluctuates from one iteration to another of the Gibbs sampler (Figure S5). Since the CG sampler converges quicker when the conditional distribution of $\boldsymbol{\beta}$ is concentrated on sparser vectors (Theorem 2.6), the number of CG iterations is highly correlated with the value of the global shrinkage parameter τ indicated by the red dotted line. With our initialization of the Gibbs sampler (Section S5.2), τ starts out small before the Monte Carlo expectation-maximization step eventually finds a value approximately maximizing the marginal likelihood. Other than the effects of fluctuation in τ , however, we can see that updating $\boldsymbol{\beta}$ requires similar numbers of CG iterations despite the randomness in $\boldsymbol{\lambda}$ and $\boldsymbol{\omega}$.

We have so far studied the mechanism of CG-acceleration by using the propensity score model example, but essentially identical conclusions follow when using the treatment effect model example. The prior preconditioning is again superior to the Jacobi one. The number of required CG iterations fluctuates along with the sparsity structure of $\boldsymbol{\beta} | \boldsymbol{\omega}, \tau, \boldsymbol{\lambda}, \mathbf{y}, \mathbf{X}$ but not significantly so after the Markov chain converges — see Figure S6, S7, and S8.

S5.2. Details on the Gibbs sampler initialization

We initialize the Gibbs samplers with the shrinkage parameter values of $\tau^{(0)} = 0.01$ and $\lambda_j^{(0)} = 1$. We then set $\boldsymbol{\omega}^{(0)}$ to the mean of its posterior distribution conditional on $\tau^{(0)}$, $\boldsymbol{\lambda}^{(0)}$, and $\beta_j^{(0)} = 0$ for all j . The parameters are then updated in the order $\boldsymbol{\beta}$, $\boldsymbol{\omega}$, τ , and $\boldsymbol{\lambda}$. In particular, the Gibbs sampler draws a state $\boldsymbol{\beta}^{(1)}$ from its posterior distribution conditional on $\boldsymbol{\omega}^{(0)}$, $\tau^{(0)}$, and $\boldsymbol{\lambda}^{(0)}$. With this initialization, all the values $\beta_j^{(1)}$'s end up being shrunk close to zero compared with their actual

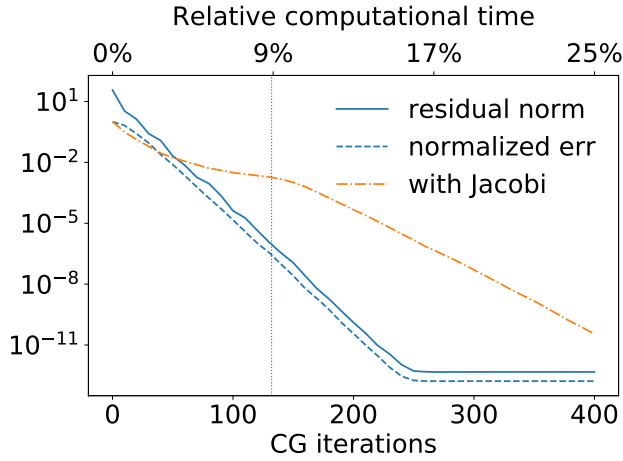


Fig. S3. Plot of the CG errors during a conditional update of β within the propensity score model posterior computation. The errors are plotted as a function of the number of CG iterations (bottom axis) and of the computational time relative to the direct linear algebra (top axis). The solid line shows the root mean squared residual $p^{-1/2}\|\tilde{\mathbf{r}}_k\|_2$ used in the stopping criteria (S2). The dotted vertical line indicates when $p^{-1/2}\|\tilde{\mathbf{r}}_k\|_2$ reaches the threshold 10^{-6} . The 2nd-moment normalized errors (S11) are shown as the blue dashed line for the prior preconditioner and as the orange dash-dot line for the Jacobi preconditioner.

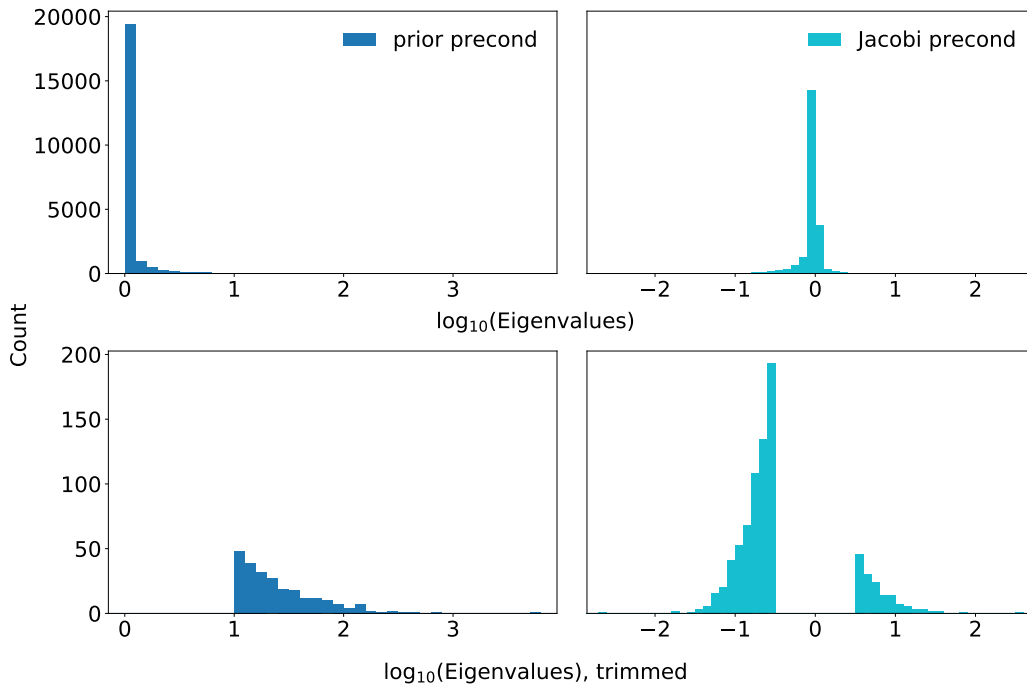


Fig. S4. Histograms of the eigenvalues of the preconditioned matrices as in Figure 3.2. The only differences here are that 1) the preconditioned matrices are based on a posterior sample from the propensity score model (4.19) and 2) the trimmed version for the Jacobi preconditioner removes the eigenvalues in the range $[-0.5, 0.5]$ as this choice better demonstrates the tail behavior here.

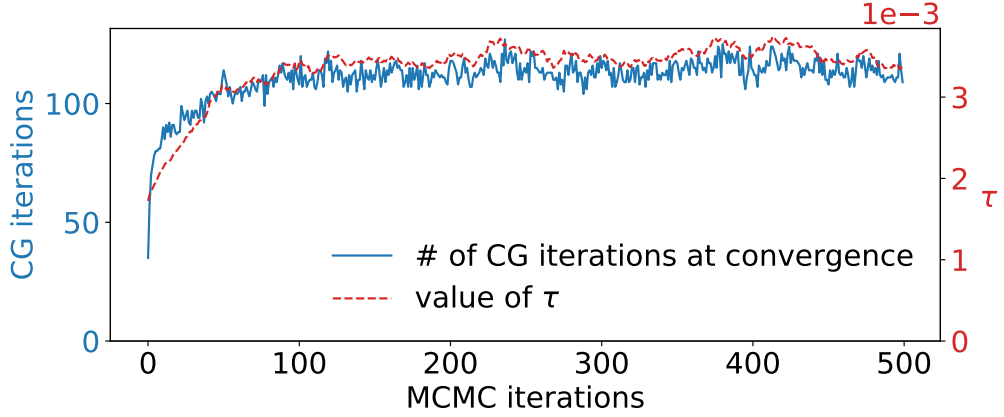


Fig. S5. Plot of the number of CG iterations required to meet the convergence criteria (S2) during each update of β by the CC-accelerated Gibbs sampler. The target distribution here comes from the propensity score model (4.19). Also shown is the value of the global shrinkage parameter τ updated via the Monte Carlo expectation-maximization steps. The value of τ significantly affect the sparsity in the conditional distribution of β and hence the number of required CG iterations.

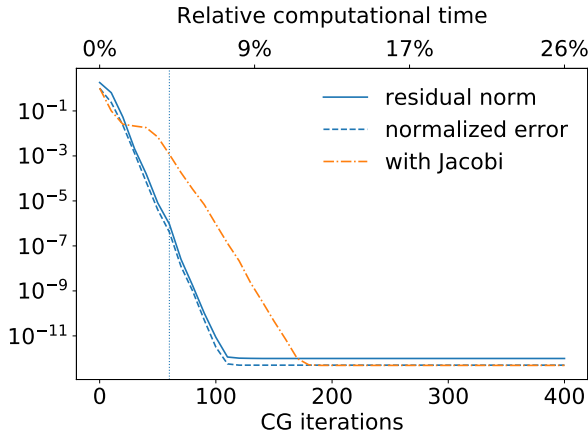


Fig. S6. Plot as in Figure S3 of the CG errors during a conditional update of β . The only difference is that the plot here is based on the treatment effect model posterior computation.

posterior means. The subsequent update of τ conditional on $\beta^{(1)}$ and $\omega^{(1)}$ (with λ marginalized out) yields $\tau^{(1)} \approx 10^{-3}$ as can be seen Figure S5. In particular, while we initialize the global shrinkage parameter value as 0.01, its value shoots down to 10^{-3} after one iteration of the Gibbs sampler. This is caused by the most components of β initially shrunk to 0, which in turn is caused by the choice $\tau^{(0)} = 0.01$ and $\lambda_j^{(0)} = 1$.

A more careful initialization of τ and λ , or alternatively of β , is likely to speed up the convergence of the Markov chain and is worth future investigations. Assessing

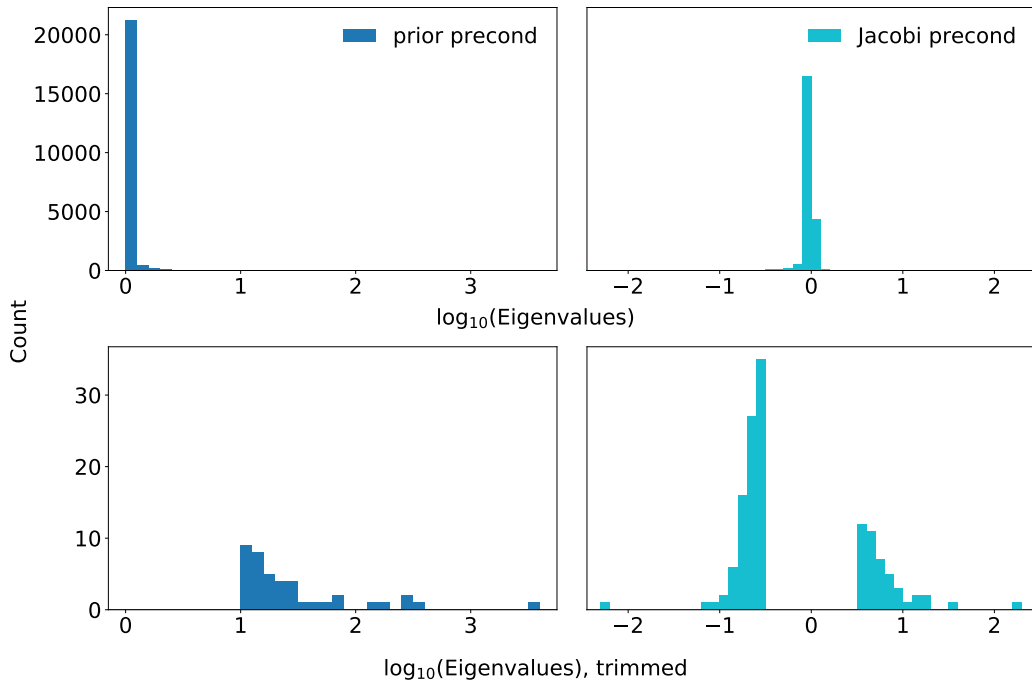


Fig. S7. Histograms of the eigenvalues of the preconditioned matrices as in Figure 3.2. The only differences here are that 1) the preconditioned matrices are based on a posterior sample from the treatment effect model (4.20) and 2) the trimmed version for the Jacobi preconditioner removes the eigenvalues in the range $[-0.5, 0.5]$ as this choice better demonstrates the tail behavior here.

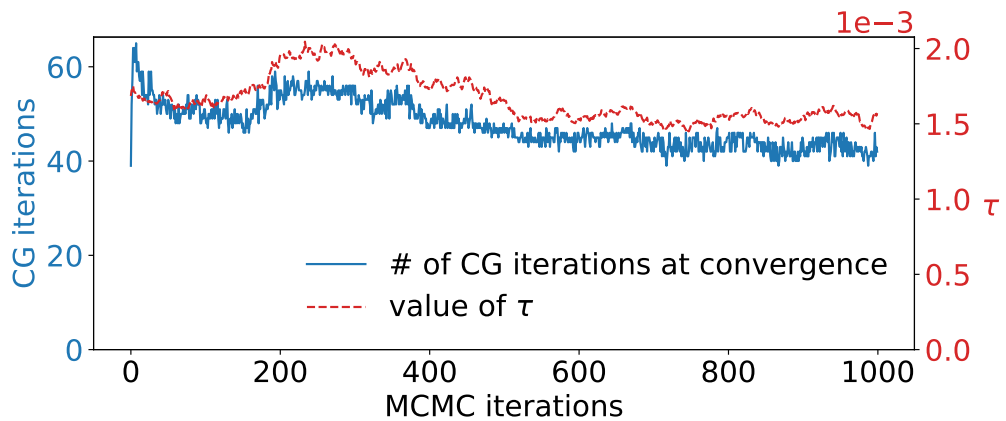


Fig. S8. Plot as in Figure S5 of the number of CG iterations required during each update of β by the CG-accelerated Gibbs sampler for the treatment effect model (4.20).

the relative importance of β_j through pre-screening techniques, such as those based on marginal correlations, may be used to initialize $\tau\lambda_j$'s.

S6. Problem with approximating $\tilde{\Phi}$ by thresholding of $\tau\lambda_j$'s

In Section 2.4, we observed that the (i, j) -th entry of $\tau^2\mathbf{\Lambda}\mathbf{X}^\top\mathbf{\Omega}\mathbf{X}\mathbf{\Lambda}$ is small whenever $\tau\lambda_i \approx 0$ or $\tau\lambda_j \approx 0$. Given this observation, one may wonder if we can obtain a convenient low-rank approximation of the prior-preconditioned matrix $\tilde{\Phi} = \tau^2\mathbf{\Lambda}\mathbf{X}^\top\mathbf{\Omega}\mathbf{X}\mathbf{\Lambda} + \mathbf{I}_p$ by zeroing out $\tau\lambda_j$'s at some threshold. This is *not* the case in general as we will show now. Intuitively, the problem is as follows: while the ordered local shrinkage parameter $\lambda_{(k)}$ decays reasonably quickly as k increases, there is no clear “gap” where $\lambda_{(k+1)} \ll \lambda_{(k)}$. For example, the histogram of a posterior draw of $\tau\lambda_j$'s in Figure 3.4 shows clearly that there is no such gap.

We can assess the quality and utility of the thresholding approximation by using it as a preconditioner for CG in solving the system $\tilde{\Phi}\tilde{\beta} = \tilde{\mathbf{b}}$. In other words, we consider using the thresholding approximation on top of prior-preconditioning. Let $(\tau^2\mathbf{\Lambda}\mathbf{X}^\top\mathbf{\Omega}\mathbf{X}\mathbf{\Lambda})_{(k)}$ denote a matrix obtained by thresholding the entries of $\tau^2\mathbf{\Lambda}\mathbf{X}^\top\mathbf{\Omega}\mathbf{X}\mathbf{\Lambda}$ to zero except for the $k \times k$ block corresponding to the k largest local shrinkage parameters $\lambda_{(1)}, \dots, \lambda_{(k)}$. Then the thresholding approximation

$$\tilde{\Phi}_{(k)} = (\tau^2\mathbf{\Lambda}\mathbf{X}^\top\mathbf{\Omega}\mathbf{X}\mathbf{\Lambda})_{(k)} + \mathbf{I}_p \quad (\text{S12})$$

is the identity perturbed by the $k \times k$ block along the diagonal. As such, using it as a preconditioner requires the one time cost of computing and factorizing the $k \times k$ block, which requires $O(k^2n + k^3)$ arithmetic operations. The quality of the approximation should improve as k increases but so does the computational cost. In particular, at some point the $O(k^2n + k^3)$ cost of preparing the thresholding preconditioner overwhelms the $O(np)$ cost of each CG iteration and becomes the computational bottleneck. When an adequate approximation requires such a large k , therefore, there is no benefit of using the thresholding approximation.

We use the example of Section 3.3 to study the effects of preconditioning the system $\tilde{\Phi}\tilde{\beta} = \tilde{\mathbf{b}}$ with the thresholding approximation $\tilde{\Phi}_{(k)}$. As before, the CG sampler is applied to the distribution (1.3) arising from the simulated data with 10 signals out of $p = 10,000$ predictors. Figure S9 shows the results for $k = 1,000, 2,000,$ and $4,000$. The convergence rates of these preconditioned CG iterations are compared to that of the CG iterations applied to the prior-preconditioned system without any additional preconditioning. If a preconditioner is a good approximation of $\tilde{\Phi}$, the preconditioned CG should yield convergence in a very small number of iterations — for example, a perfect approximation would induce the convergence after one iteration. It is clear from Figure S9, however, that the thresholding approximation does more harm than good in terms of the CG convergence rate, especially when k is taken small relative to the size of $\tilde{\Phi}$. We can therefore conclude that the thresholding strategy yields a poor approximation except when k starts to become almost as large as p .

We repeated the same experiments on the thresholding approximation $\tilde{\Phi}_{(k)}$ using the other posterior distributions discussed in the manuscript. Across the exper-

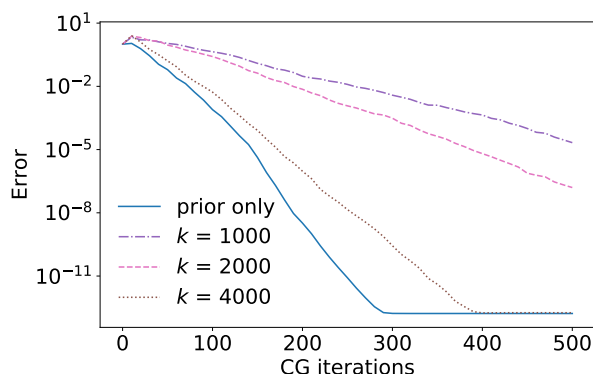


Fig. S9. Plot of the CG approximation errors (with the same error metric as used in Figure 3.1) as a function of the number of CG iterations. The CG sampler here is applied to the conditional distribution of β arising from the simulated data example with 10 signals as described in Section 3. Each line corresponds to a different threshold level k for the approximation (S12). The blue line labeled ‘prior only’ corresponds to CG applied to the prior preconditioned system without any further preconditioner.

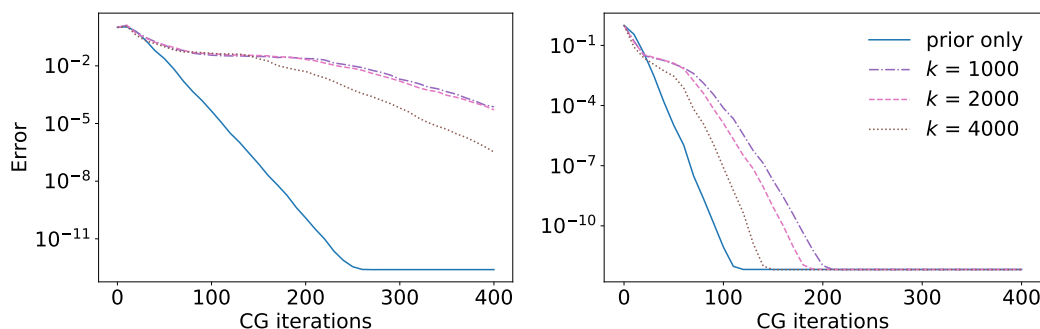


Fig. S10. Plots of the CG approximation errors (with the same error metric as used in Figure 3.1) as a function of the number of CG iterations. The CG samplers are applied to the conditional distribution of β arising from the propensity score model (4.19) (the left plot) and treatment effect model (4.20) (the right plot).

iments, no computational gain could be achieved by using the thresholding approximation as a preconditioner. More precisely, to yield a good enough approximation, the value of k had to be so large that preparing the preconditioner itself became a computational bottleneck. The convergence rates of CG preconditioned by the thresholding approximation are shown in Figure S10 for the dabigatran and warfarin comparison examples of Section 4. This real data example again confirms the poor quality of the thresholding approximation.

References for Supplement

- Azad, A., Ballard, G., Buluc, A., Demmel, J., Grigori, L., Schwartz, O., Toledo, S. and Williams, S. (2016) Exploiting multiple levels of parallelism in sparse matrix-matrix multiplication. *SIAM Journal on Scientific Computing*, **38**, C624–C651.
- Bank, R. E. and Douglas, C. C. (1993) Sparse matrix multiplication package (smmp). *Advances in Computational Mathematics*, **1**, 127–137.
- Davis, T. A. (2011) Algorithm 915, SuiteSparseQR: Multifrontal multithreaded rank-revealing sparse QR factorization. *ACM Transactions on Mathematical Software (TOMS)*, **38**, 8.
- Dongarra, J., Heroux, M. A. and Luszczek, P. (2016) High-performance conjugate-gradient benchmark: A new metric for ranking high-performance computing systems. *The International Journal of High Performance Computing Applications*, **30**, 3–10.
- Duff, I. S., Erisman, A. M. and Reid, J. K. (2017) *Direct methods for sparse matrices*. Oxford University Press.
- Duff, I. S., Heroux, M. A. and Pozo, R. (2002) An overview of the sparse basic linear algebra subprograms: The new standard from the BLAS technical forum. *ACM Transactions on Mathematical Software (TOMS)*, **28**, 239–267.
- Matam, K., Indarapu, S. R. K. B. and Kothapalli, K. (2012) Sparse matrix-matrix multiplication on modern architectures. In *19th International Conference on High Performance Computing (HiPC)*, 1–10. IEEE.
- Park, T. and Casella, G. (2008) The Bayesian Lasso. *Journal of the American Statistical Association*, **103**, 681–686.
- Rue, H. and Held, L. (2005) *Gaussian Markov random fields: theory and applications*. CRC press.
- Saad, Y. (2011) *Numerical Methods for Large Eigenvalue Problems: Revised Edition*. Classics in Applied Mathematics. Society for Industrial and Applied Mathematics.
- Zucknick, M., Saadati, M. and Benner, A. (2015) Nonidentical twins: comparison of frequentist and Bayesian lasso for Cox models. *Biometrical Journal*, **57**, 959–981.